Journal of Controlled Release 332 (2021) 594–607

Contents lists available at ScienceDirect

Journal of Controlled Release

journal homepage: www.elsevier.com/locate/jconrel

Matrix metalloproteinase-1 decorated polymersomes, a surface-active extracellular matrix therapeutic, potentiates collagen degradation and attenuates early liver fibrosis

Eline Geervliet [a,1], Silvia Moreno [b,1], Luca Baiamonte [b], Richell Booijink [a], Susanne Boye [b], Peng Wang [b,c], Brigitte Voit [b,c], Albena Lederer [b,d,**], Dietmar Appelhans [b,1,**], Ruchi Bansal [a,*,1]

[a] Translational Liver Research, Department of Medical Cell Biophysics, Technical Medical Centre, Faculty of Science and Technology, University of Twente, Drienerlolaan 5, 7522 NB Enschede, the Netherlands
[b] Leibniz-Institut für Polymerforschung Dresden e.V., Hohe Straße 6, 01069 Dresden, Germany
[c] Technische Universität Dresden, Organic Chemistry of Polymers, 01062 Dresden, Germany
[d] Department of Chemistry and Polymer Science, Stellenbosch University, Matieland 7602, South Africa

ARTICLE INFO

Keywords:
Surface-active polymersomes
Structure and storage properties
Extracellular matrix degrading therapeutic
Matrix metalloproteinase-1
Liver fibrosis

ABSTRACT

Liver fibrosis affects millions of people worldwide and is rising vastly over the past decades. With no viable therapies available, liver transplantation is the only curative treatment for advanced diseased patients. Excessive accumulation of aberrant extracellular matrix (ECM) proteins, mostly collagens, produced by activated hepatic stellate cells (HSCs), is a hallmark of liver fibrosis. Several studies have suggested an inverse correlation between collagen-I degrading matrix metalloproteinase-1 (MMP-1) serum levels and liver fibrosis progression highlighting reduced MMP-1 levels are associated with poor disease prognosis in patients with liver fibrosis. We hypothesized that delivery of MMP-1 might potentiate collagen degradation and attenuate fibrosis development. In this study, we report a novel approach for the delivery of MMP-1 using **MM**P-1 decorated **p**olymer**somes** (MMPsomes), as a surface-active vesicle-based ECM therapeutic, for the treatment of liver fibrosis. The storage-stable and enzymatically active MMPsomes were fabricated by a post-loading of Psomes with MMP-1. MMPsomes were extensively characterized for the physicochemical properties, MMP-1 surface localization, stability, enzymatic activity, and biological effects. Dose-dependent effects of MMP-1, and effects of MMPsomes *versus* MMP-1, empty polymersomes (Psomes) and MMP-1 + Psomes on gene and protein expression of collagen-I, MMP-1/TIMP-1 ratio, migration and cell viability were examined in TGFβ-activated human HSCs. Finally, the therapeutic effects of MMPsomes, compared to MMP-1, were evaluated *in vivo* in carbon-tetrachloride (CCl_4)-induced early liver fibrosis mouse model. MMPsomes exhibited favorable physicochemical properties, MMP-1 surface localization and improved therapeutic efficacy in TGFβ-activated human HSCs *in vitro*. In CCl_4-induced early liver fibrosis mouse model, MMPsomes inhibited intra-hepatic collagen-I (ECM marker, indicating early liver fibrosis) and F4/80 (marker for macrophages, indicating liver inflammation) expression. In conclusion, our results demonstrate an innovative approach of MMP-1 delivery, using surface-decorated MMPsomes, for alleviating liver fibrosis.

1. Introduction

Liver fibrosis is an abnormal wound healing process, which upon chronic injury, results in an accumulation of collagenous-rich extracellular matrix (ECM) and progresses to liver cirrhosis and/or hepatocellular carcinoma [1]. Among others, viral infections, excessive alcohol/drug abuse and metabolic disorders are the major etiologies causing liver-related pathologies [2]. Liver fibrosis affects millions of people worldwide [3] and is rising vastly over the past decades, mainly due to unhealthy and sedentary lifestyle [4,5]. With no viable therapies

* Corresponding authors.
** Corresponding author at: Leibniz-Institut für Polymer Polymerforschung Dresden e.V., Hohe Straße 6, 01069 Dresden, Germany.
E-mail addresses: lederer@ipfdd.de (A. Lederer), applhans@ipfdd.de (D. Appelhans), r.bansal@utwente.nl (R. Bansal).
[1] Equal contribution.

https://doi.org/10.1016/j.jconrel.2021.03.016
Received 2 November 2020; Received in revised form 8 March 2021; Accepted 12 March 2021
Available online 15 March 2021

available, organ transplantation is the only curative treatment for advanced diseased patients [6]. However, with increasing demands of donor livers and inherent challenges associated with liver transplantation, there is an urgent need for the development of more effective therapies [7].

Injury to the liver induces processes (Fig. 1) leading to the activation of resident quiescent hepatic stellate cells (HSCs) [8]. Upon activation, quiescent HSCs undergo trans-differentiation into proliferative and pro-fibrogenic myofibroblasts that secrete excessive ECM components, mainly collagen-I (col-I), thereby resulting in scarring, loss-of-liver architecture and function [9]. ECM homeostasis is mainly regulated by matrix metalloproteinases (MMPs) and tissue inhibitors of MMPs (TIMPs) [10,11]. The MMP-TIMP balance is dysregulated during liver injury, with decreased MMPs and increased TIMPs, resulting in reduced matrix degradation while increased ECM production by activated HSCs [5,7]. Besides liver diseases, MMPs are also implicated in other inflammatory and fibrotic diseases including arthritis, cardiovascular disorders, cancer and metastasis [12].

The first discovered MMP, MMP-1 or collagenase-1 binds to and cleaves col-I, the most abundant ECM protein present in the fibrotic livers [13]. Several studies have suggested an inverse correlation between serum MMP-1 levels and liver fibrosis progression highlighting that reduced MMP-1 levels are associated with poor disease prognosis in patients with liver fibrosis [14,15]. Since MMP-1 is the most potent collagenase that can degrade fibrillar collagens [16,17], its therapeutic effect is widely studied. Iimuro et al. investigated MMP-1 delivery using adenoviral-vector mediated human pro-MMP-1 (Ad5MMP-1) in thioacetamide (TAA)-induced fibrotic rats. Ad5MMP-1 increased the active MMP-1 levels, degraded the fibrous ECM, induced apoptosis of activated HSCs and attenuated fibrosis [18]. Du et al. augmented MMP-1 expression *via* transplantation of MMP-1 overexpressing bone-marrow-derived stem cells (BMSCs) in carbon tetrachloride (CCl_4)-induced fibrotic rats and demonstrated decreased col-I expression, HSCs inhibition and amelioration of liver fibrosis [19]. Other studies have focused on inducing MMP-1 expression using different compounds [20,21]. These studies clearly demonstrate the importance of MMP-1 delivery for the treatment of liver fibrosis. Despite promising findings, MMP-1 delivery using adeno-viral vectors may lead to adverse effects [22] and/or BMSCs possess inherent challenges including invasive BMSCs isolation procedure and poor BMSCs survival [23,24]. These problems can be overcome by delivery of MMP-1 using polymersomes (Psomes) as a drug delivery system (DDS).

In the past two decades, Psomes have attracted growing attention as polymeric vesicles mimicking cell- and virus-dimensions, and as DDS for medical applications [25–31]. Due to their defined aqueous compartments, Psomes can encapsulate proteins in the lumen protected, by the membrane, against (enzymatic) degradation in the biological environment, thus functioning as feedback-controlled or enzymatic nanoreactors [32–37]. Moreover, stimuli-sensitive Psomes have emerged as novel programmable delivery systems in which the release of encapsulated contents can be readily modulated by internal/external stimuli, preferentially through the disassembly of Psomes, or using transmembrane proteins. These DDSs significantly enhanced therapeutic efficacy and minimized possible adverse effects [31,38–41]. However, to date, there are no studies on surface-attached proteins or membrane-integrated proteins in Psomes, and their suitability to be used as surface-active polymeric vesicle therapeutics in the ECM-rich fibrotic microenvironment. Furthermore, the formation of such selectively modified Psomes and their potential as DDS remain largely unexplored. The aim of this study is to design novel ECM therapeutics based on enzymatically active, surface-modified **MM**P-1 **Psomes** (MMPsomes) to treat liver fibrosis (Fig. 1).

This study demonstrates a novel enzymatic therapeutic approach (Fig. 1) for the direct degradation of col-I in the ECM thereby attenuating liver fibrosis. This approach is based on MMPsomes designed as biologically surface-active vesicle-based DDS that undoubtedly differ from reported enzyme/protein loaded Psomes [28–30,40,42], where intracellular delivery of proteins is not imperative. We postulate that MMPsomes stabilizes MMP-1 which then efficiently degrades col-I, inhibits HSCs-induced col-I expression and enhances relative MMP-1/TIMP-1 expression thereby ameliorating liver fibrosis (Fig. 1).

2. Materials and methods

2.1. Materials

All materials were used as received, unless stated otherwise. Collagenase type I (also referred to as MMP-1), prepared from *Clostridium histolyticum*, Sigma-Aldrich, C0130-100 mg, CAS no. 9001–12-1; collagenase activity colorimetric assay kit MAK293 containing collagenase assay buffer MAK293A, collagenase MAK293B, collagenase substrate MAK293C (FALPGA – *i.e.* a modified synthetic peptide), inhibitor MAK293D (1,10-phenanthroline 1 M); phosphate buffered saline (PBS) tablets (Sigma-Aldrich); sodium azide (NaN_3) (Sigma-Aldrich); 37%

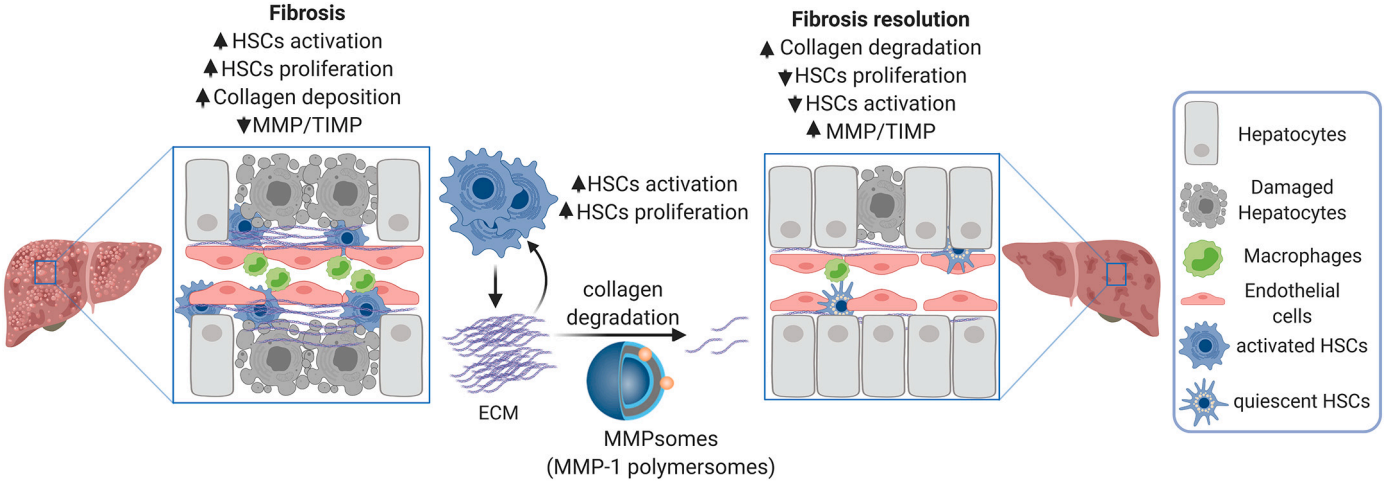

Fig. 1. Schematic illustration of an approach using MMPsomes for liver fibrosis resolution. During chronic liver injury, hepatocytes undergo apoptosis and necrosis releasing pro-inflammatory and pro-fibrotic factors. These factors induce infiltration and activation of macrophages causing liver inflammation, followed by proliferation and activation of HSCs that secrete excessive amounts of fibrotic ECM, primarily collagen-I. Degradation of collagen-I, by a surface active MMP-1-decorated polymersomes (MMPsomes), can restore balance between ECM deposition and degradation, and thereby favor resolution of liver fibrosis. Created with BioRender.com.

hydrochloric acid (HCl) (Merck); sodium hydroxide (NaOH) (Sigma-Aldrich). The BCPs (refer to Table S1) have been prepared by atom transfer radical polymerization (ATRP). The hydrophilic part displays a methoxy group at the end of a PEG segment, while the hydrophobic part consists of pH-sensitive 2-(N,N′-diethylamino)ethyl methacrylate (DEAEMA) and photo-crosslinker 3,4-dimethyl maleic imidobutyl methacrylate (DMIBM). The composition and the number average molecular weight (M_n) of the block copolymer were determined with ^1H nuclear magnetic resonance (NMR) spectroscopy from the peak integrals of PEG (3.65 ppm), DEAEMA (2.65–2.78 ppm) and DMIBM (3.52 ppm) by taking the PEG block as an internal standard. BCP: PEG_{45}-b-($DEAEMA_{91}$-s-$DMIBM_{24}$).

2.2. Fabrication of polymersomes (Psomes), MMP-1-decorated Psomes (MMPsomes) and MMP-1

Empty polymersomes (Empty-Psomes). The assembly of empty Psomes was carried out by dissolving the BCP in HCl 0.01 M (pH 2.0) at a concentration of 1 mg/mL. The solution was then passed through a 0.2 μm nylon filter to remove all the impurities. Next, pH was increased from 2.0 to 5.0 by addition of 1 M NaOH and then to 9.0 with 0.1 M NaOH. The suspension was then left stirring in the dark for 72 h and passed through a 0.8 μm nylon filter. Crosslinking of Psomes was carried out for 180 s per 2 mL of suspension using a UV crosslink lamp, Omni-Cure S2000 UV curing lamp system (Lumen Dynamics Group Inc., Canada) equipped with high pressure mercury lamp (0.35 W/cm^2, UV light between 320 and 500 nm). After crosslinking, the swelling behaviour, size, polydispersity index (PDI) and zeta potential of the Psomes were analyzed using batch dynamic light scattering (DLS).

Post-loaded MMP-1-polymersomes (MMPsomes). A stock solution of 0.2 mg/mL collagenase-I (MMP-1) was prepared by dissolving the enzyme in 1 mM PBS and stirring overnight. This solution was mixed with a suspension of empty Psomes (prepared as described above) in 1:1 ratio to obtain the following concentrations: C_{BCP} = 0.5 mg/mL and $C_{MMP\text{-}1}$ = 0.1 mg/mL. The pH of the resulting solution was adjusted to a value of 5.0 by addition of 0.1 M HCl. The suspension was left stirring in the dark overnight. Finally, the pH was adjusted to a value of 9.0 by addition of 0.1 M NaOH. Synthesized MMPsomes were purified using optimized protocols as described below, the swelling behaviour, size, PDI, and zeta potential of MMPsomes were assessed using batch DLS and asymmetric flow field-flow fractionation (AF4) with light scattering (AF4-LS).

For the biomedical experiments (cell viability and therapeutic efficacy): A stock solution of 0.4 mg/mL MMP-1 was prepared by dissolving the enzyme in 1 mM PBS at pH 6.0. This solution was mixed to a suspension of empty Psomes, pH 6.0 (prepared as described above) in 1:1 ratio to obtain the following concentrations: C_{BCP} = 0.5 mg/mL and $C_{MMP\text{-}1}$ = 0.2 mg/mL.

Free MMP-1. Solutions of free enzyme were prepared by dissolving collagenase/MMP-1 in 1 mM PBS at a concentration of 0.2 mg/mL. Solutions were stirred slowly for at least 2 h before using for further studies.

2.3. Dialysis and HFF purification of unpurified post-loaded MMPsomes

(a) Dialysis was carried out against 1 mM PBS for 72 h in the dark (membrane MWCO: 1000 kDa) to remove all free MMP-1 biomacromolecules from "Unpurified MMPsomes". During this time, the buffer was changed daily and kept on constant stirring. Dialysis-purified MMPsomes (Dialysis MMPsomes) were used for batch DLS and AF4 study as well as for examining different storage methods.

(b) Hollow Fiber Filtration (HFF) was carried out using KrosFlo Research System equipped with a hydrophilic-modified poly (ethersulphone) membrane (500 kDa, SpectrumLabs, USA). The transmembrane pressure (TMP) was set to 130 mbar. A 15 mL/min flow of 1 mM PBS (pH 8.0) was used to remove free MMP-1 biomacromolecules: several cycles were performed; until 120 mL of buffer were obtained as permeate. According to the preliminary studies, all the free MMP-1 biomacromolecules were eliminated from the suspension. This was confirmed by enzymatic activity assay of the last fraction of permeate. HFF-purified MMPsomes (HFF MMPsomes) were used for batch DLS and AF4 study as well as for examining different storage methods.

2.4. Fluorescence study

Preparation of Na_2CO_3/$NaHCO_3$ buffer at pH 10.0. 1.12 g of Na_2CO_3 was dissolved in 100 mL Milli-Q water, separately, 1.68 g of $NaHCO_3$ was also dissolved in 100 mL Milli-Q water. 3.5 mL of the Na_2CO_3 solution was mixed with 2.8 mL of $NaHCO_3$ solution and Milli-Q water was added to reach a volume of 100 mL, resulting in a Na_2CO_3/$NaHCO_3$ buffer pH 10.

Synthesis of MMP-1-RhB: 5 mg (0.05 μmol, equivalent 1) of MMP-1 was dissolved in 3 mL of carbonate buffer at pH 10, later 9.65 μL of DMSO containing 0.168 mg RhB-SCN (0.3 μmol, equivalent 6) was added. This was stirred for 2 days and extensively dialyzed against 1 mM PBS using a 2 kDa MWCO membrane for 2 days (C_{Stock} = 1 mg/mL), continuously changing the buffer.

Fabrication of labeled MMPsomes: 1 mL of MMP-1-RhB solution (1 mg/mL) was dissolved in 4 mL PBS at pH 6, to this solution; 5 mL of Psomes (1 mg BCP/mL Psomes) at pH 6 was added and stirred overnight (C_{BCP} = 0.5 mg/mL and $C_{MMP\text{-}1\text{-}RhB}$ = 0.1 mg/mL). The sample was studied using two purification methods: (a) the sample was extensively dialyzed to 1 mM PBS pH 7.4, for 3 days, using a 1000 kDa MWCO membrane. Samples were taken after 0, 8, 24, 48 and 72 h. The samples were prepared and analyzed by triplicate; (b) The sample was purified by HFF (130 mbar, 150 mL waste, 500 kDa, 1 mM PBS pH 7.4) Samples were taken before and after purification. The samples were prepared and analyzed by triplicate (C_{BCP} = 0.25 mg/mL, λ_{ex} = 554 nm, λ_{abs} = 575 nm). *As a control*, the fluorescence intensity of free MMP-1-RhB without dialysate was studied after 1, 2, 3 and 4 days ($C_{MMP\text{-}1\text{-}RhB}$ = 0.1 mg/mL, λ_{ex} = 554 nm, λ_{abs} = 575 nm).

For the biomedical experiments, 2 mL of MMP-1-RhB solution (1 mg/mL) was dissolved in 3 mL PBS at pH 6, to this solution; 5 mL of Psomes (1 mg BCP/mL Psomes) at pH 6 was added to MMP-1-RhB solution and stirred overnight (C_{BCP} = 0.5 mg/mL and $C_{MMP\text{-}1\text{-}RhB}$ = 0.2 mg/mL) and purified by dialysis.

2.5. Determination of pH

(A) MMPsomes or Empty-Psomes (C_{BCP} = 0.25 mg/mL and $C_{MMP\text{-}1}$ = 0.05 mg/mL) in buffer assay (50 mM Tricine with 10 mM Calcium Chloride and 400 mM Sodium Chloride). (B) MMPsomes or Empty-Psomes (C_{BCP} = 0.25 mg/mL and $C_{MMP\text{-}1}$ = 0.05 mg/mL) in 1 mM PBS. Post-loading method was used for preparing MMPsomes, purified by dialysis. Both MMPsomes and Empty-Psomes were titrated from basic to acidic conditions while simultaneously measuring their size by dynamic light scattering (DLS) by adding of HCl 0.1 M to determine the pH.

2.6. Fluorescence resonance energy transfer (FRET)

For a solution of Avidin.AlexaFluor488-Psomes (0.25 mg BCP/mL, V = 10 mL) the pH was adjusted to pH 6 and then, 60 μL of HABA (fresh solution, 1 mg/mL) was added. The sample was stirred for 2 h. The samples before and after adding HABA were used as reference (triplicate) to check the right quenching (100 μL per well). Subsequently, 0.25 mg/mL Avidin.AlexaFluor488.HABA-Psomes solution were prepared in 1 mM PBS at different pH (8, 7 and 6; enzyme assay buffer) and setting in 96 well plate (100 μL per well). Later, the biotinylated peptide FALGPA was added. After 6 h, All samples were adjusted at pH 6 adding 100 μL of 10 mM PBS at pH 6 were added per well to study the fluorescence

intensity. All samples were analyzed at 0.25 mg BCP/mL by fluorescence microscopy using a microplate reader at λ_{ex}: 488 nm.

2.7. MMPsomes storage

Here, two different storage methods were compared: (a) *Cryogenic freezing (frozen)*, the samples were kept overnight in a freezer at −20 °C in the dark. On the next day, the samples were thawed for at least 2 h before being characterized; (b) *Freeze-drying (FD),* before the process 0.1% *w/v* inulin was added to the samples as cryo-protectant. The samples were then frozen by liquid nitrogen and freeze-dried overnight in the dark at a pressure of 0.030 mbar. On the next day, the solid obtained by this process was directly dissolved in 1 mM PBS at pH 5, stirring, for at least 2 h.

Once the loaded and purified Psomes were prepared, MMPsomes were stored for 7 days at 4 °C to carry out the corresponding biological studies. The influence on the enzyme activity over the days was studied at 1, 3 and 7 days. Both conditions were used: (a) C_{BCP} = 0.5 mg BCP/mL + 0.2 mg MMP-1/mL. Psomes aliquots (C_{BCP} = 0.5 mg BCP/mL) were stored at −20 °C up to several weeks for preparing MMPsomes as described above.

2.8. Enzymatic assay for MMPsomes

The collagenase activity colorimetric assay kit (MAK293, Sigma) was used for the determination of MMP-1 activity as per manufacturer's instructions. Briefly, a reaction mixture was prepared by combination of assay buffer with substrate (FALGPA) using a volume ratio of 60:40. For the analysis, 100 μL of MMPsomes were added to the microwell of a 96-well plate. Just before starting the measurement, 100 μL of reaction mixture were added to each microwell. Measurements were carried out on a Tecan microplate reader at λ = 345 nm, 37 °C. Enzyme activity was measured 4–5 days after the fabrication of MMPsomes. Every sample was measured in triplicate. The background (negative) control was constituted by 100 μL of assay buffer, while the positive control consisted in 10 μL assay MMP-1 and 90 μL assay buffers. Absorbance was measured every 30 s for a total time of 15 min. The enzymatic activity of (MMPsomes) samples was calculated as described in the kit's technical bulletin.

2.9. Stability studies of MMPsomes and assessment of MMP-1 leakage from MMPsomes

Stability studies of Empty-Psomes and Dialysis MMPsomes in 1 mM PBS, 10% FBS in mM PBS and serum-free DMEM: Dialysis MMPsomes, prepared for biological experiments ($C_{Empty\text{-}Psomes}$ = 0.25 mg BCP/ mL and $C_{MMP\text{-}1}$ = 0.1 mg/mL), and Empty-Psomes ($C_{Empty\text{-}Psomes}$ = 0.25 mg BCP/mL) were incubated at 37 °C in three different solutions: a) 1 mM PBS, b) 10% FBS in 1 mM PBS and c) serum-free DMEM medium. All samples were analyzed by DLS after different time points of incubation (0, 2, 4, 6, 8, 24 and 48 h).

Assessment of MMP-1 leakage from Dialysis MMPsomes after 3 pH cycles: 9 mL of purified MMPsomes using MMP-1-RhB (reference: 100%, MMPsomes purified by dialysis for 72 h using MMP-1-RhB, 0.5 mg BCP/mL) were incubated at pH 6 for 15 min, afterwards the pH was adjusted to pH 7.5 (1 cycle). 3 mL of this solution was taken and dialyzed against 1 mM PBS for 24 h. The same procedure was repeated two more times (2 and 3 cycles). The absorbance of all samples was measured at 556 nm and presented as percentage (%) MMP-1 in MMPsomes.

2.10. Cell line

LX-2, an immortalized human HSC cell line used in this study was provided by Prof. Scott Friedman (Mount Sinai Hospital, New York, NY, USA). The cells were cultured in Dulbecco's modified Eagle's medium (DMEM) containing 10% fetal bovine serum (FBS, Lonza, Verviers, Belgium), 1% L-glutamine and 1% penicillin/streptomycin (pen/strep) (Sigma Aldrich). The cells were passaged twice a week as per established experimental protocols.

2.11. Cell viability studies

Cells were seeded in 12-well plates (1×10^5 cells/well/mL) and cultured overnight. Cells were serum-starved for overnight and incubated with starvation medium alone, different concentrations of MMP-1 (0.25, 0.5, 1.0 and 5.0 μg/mL), MMP-1 + Psomes, MMPsomes (MMP-1 conc. of 1.0 μg/mL and respective Psomes concentration of 4.17 μg/mL) and Psomes (4.17 μg/mL) for 24 h. Cells were then incubated with Alamar blue reagent (Invitrogen, Carlsbad, CA, USA) for 4 h and fluorescent signal of the medium was measured using a VIKTOR™ plate reader (Perkin Elmer, Waltham, MA).

2.12. Quantitative real-time PCR

Cells were seeded in 12-well cell culture treated plates (1×10^5 cells/well/mL) and cultured overnight. Cells were then serum-starved for overnight and incubated with starvation medium alone, equivalent concentrations (1.0 μg/mL) of MMP-1, Psomes, MMP-1 + Psomes and MMPsomes, and 5 ng/mL TGFβ for 24 h. Cells were then lysed using RNA lysis buffer and total RNA was isolated using the GenElute Total RNA Miniprep Kit (Sigma) according to the manufacturer's instructions. The RNA concentration was quantified using NanoDrop® ND-1000 Spectrophotometer (Thermo Scientific, Waltham, USA). Total RNA (1 μg) was reverse transcribed using the iScript cDNA Synthesis Kit (Bio-Rad, Hercules, CA, USA). Real-time PCR was performed using 20 ng of cDNA, pre-tested gene-specific primer sets as listed below in Table 1 and the 2× SensiMix SYBR and Fluorescein Kit (Bioline GmbH, QT615–05, Luckenwalde, Germany) according to the manufacturer's instructions. Finally, cycle threshold (Ct) values were normalized to the reference gene 18 s rRNA, and relative expressions were calculated using the 2-ΔΔCt method *versus* TGFβ-treated LX2 cells.

2.13. Western blot analysis

Cells were seeded in 12-well plates (1×10^5 cells/well/mL) and cultured overnight. Cells were serum-starved for overnight and incubated with starvation medium alone, equivalent concentrations (1.0 μg/mL) of MMP-1, Psomes, MMP-1 + Psomes and MMPsomes, and 5 ng/mL TGFβ for 48 h. Cells were then lysed using 1× lysis buffer prepared from 3× blue loading buffer and 30× reducing agent (1.25 M dithiothreitol, DTT) (Cell Signaling Technology, Massachusetts, MA, USA) as per manufacturer's instructions. The prepared samples were loaded on 10% Tris-glycine gels (Life Technologies) followed by transfer to the PVDF membrane (Roche). The membranes were developed according to the standard protocols using primary antibodies *i.e.*, polyclonal goat anti-collagen-I (1:500, Southern Biotech) and mouse monoclonal β-actin antibody (1:5000, Sigma) and respective secondary antibodies (Dako). The bands were visualized using Pierce™ ECL Plus Western Blotting substrate (Thermo Scientific, Rockford, IL, USA) and photographed using FluorChem Imaging System. Intensity of individual bands was quantified using NIH ImageJ software, normalized with respective β-actin bands and presented as relative expression *versus* TGFβ-treated LX2 cells.

2.14. Solid phase Sandwich enzyme-linked Immunosorbent assay (ELISA)

Cells were seeded in 12-well plates (1×10^5 cells/well/mL) and cultured overnight. Cells were serum-starved for overnight and incubated with starvation medium alone, equivalent concentrations (1.0 μg/mL) of MMP-1, Psomes, MMP-1 + Psomes and MMPsomes, and 5 ng/mL TGFβ for 48 h. Culture supernatant was collected, diluted 1:5 in diluent

Table 1
Sequence of the human primers used for quantitative real-time PCR:

Gene	Forward primer (5′-3′)	Reverse primer (5′-3′)	Accession no.
Col1a1	GTACTGGATTGACCCCAACC	CGCCATACTCGAACTGGAAT	NM_000088.3
TIMP-1	GGGGACACCAGAAGTCAACC	GGGTGTAGACGAACCGGATG	NM_003254.2
MMP-1	TGGTGTCTCACAGCTTCCCA	CTCCACATCTGGGCTGCTTC	NM_002421.3
18s rRNA	TGAGGTGGAACGTGTGATCA	CCTCTATGGGCCCGAATCTT	NM_022551.2

(1% BSA in PBS), and 5 μL was used to analyze secreted collagen-I using Human Pro-Collagen I alpha 1 DuoSet® ELISA (DY6220–05, R&D systems) as per manufacturer's instructions. The optical density was measured at 450 nm using VIKTOR™ plate reader (Perkin Elmer). Concentration of the secreted collagen-I was calculated using the standard curve.

2.15. Cell migration study

Cells were plated in 12-well culture plates (1×10^5 cells/well/1 mL), cultured overnight and serum-starved for 24 h. A standardized scratch was made using a 200 μL pipette tip fixed in a custom-designed holder. Afterwards, cells were washed twice and incubated with starvation medium (control), or with 5 ng/mL TGFβ without or with equivalent concentrations (1.0 μg/mL) of MMP-1, Psomes, MMP-1 + Psomes and MMPsomes. Microscopic images were taken at 0 and 24 h to measure the size of the scratch. Photographs were analyzed using NIH ImageJ software, normalized with 0 h time point and presented as % relative wound healing *versus* TGFβ-treated LX2 cells.

2.16. 3D collagen matrix degradation study

A collagen suspension (5 mL) was prepared containing 3 mL of collagen G1 (5 mg/mL, Matrix biosciences, Morlenbach, Germany), 0.5 mL of 10× M199 medium (Sigma), 85 μL of 1 N NaOH (Sigma) and sterile water. This collagen suspension was mixed with 1 mL (2×10^6) of LX2 cells. 600 μL of gel-cell suspension was plated in a 24-well plated and incubated 1 h at 37 °C for polymerization. Polymerized gels were incubated with 1 mL of starvation medium alone (control), MMP-1 (1.0 μg/mL), and MMPsomes (1.0 μg/mL), for 48 h. Images were made using a digital camera. The size of the gels was measured using NIH ImageJ software and normalized to their respective well size, representing the degradation of collagen matrix.

2.17. In vivo study

CCl_4-induced early liver fibrogenesis mouse model: All the animal experiments were carried out according to the ethical guidelines for the Care and Use of Laboratory Animals (Utrecht University, The Netherlands). Male C57BL/6 mice (8–10 weeks old) were given as a single intraperitoneal injection of 1.0 mL/kg carbon tetrachloride (CCl_4, Sigma) as described previously [43–46]. Only male mice were used, since female hormones can affect the fibrosis progression resulting in variations. After 48 h of CCl_4 administration, single intravenous administration of PBS ($n = 5$), MMP-1 (10 μg/mice/dose, $n = 4$) or MMPsomes (10 μg MMP-1 + 41.7 μg Psomes/mice/dose, n = 5) were given. Healthy controls (n = 5) received olive oil alone. After 24 h of treatment, all the animals were euthanized. All the animals and liver tissues were weighed, and liver tissues were used for further analyses.

2.18. Histological immunostainings

Collected liver tissues were transferred to Tissue-Tek OCT embedding medium (Sakura Finetek, Torrance, CA, USA) and snap-frozen in 2-methyl butane in a dry ice. Cryosections (5 μm) were cut using a Leica CM 3050 cryostat (Leica Microsystems, Nussloch, Germany). The cryosections were air-dried and fixed with acetone for 20 min. Tissue sections were rehydrated with PBS and incubated with the primary antibody *i.e.*, polyclonal goat anti-collagen I (1:100, Southern Biotech) or rat monoclonal anti-F4/80 (1:100, BioRad) overnight at 4 °C. This was followed by incubation with horseradish peroxidase (HRP)-conjugated secondary antibodies (Dako) for 1 h at RT. Next, the samples were incubated with HRP-conjugated tertiary antibodies (Dako) for 1 h at RT. Thereafter, peroxidase activity was developed using the AEC (3-amino-9-ethyl carbazole) substrate kit (Life Technologies) for 20 min and nuclei were counterstained with hematoxylin (Fluka Chemie, Buchs, Switzerland). Endogenous peroxidase activity was blocked by 3% H_2O_2 prepared in methanol. The sections were mounted with Aquatex mounting medium (Merck) and were scanned using Hamamatsu NanoZoomer Digital slide scanner 2.0HT (Hamamatsu Photonics).

2.19. Graphs and statistical analyses

All the graphs were made using GraphPad Prism version 8.4.2 (GraphPad Prism, La Jolla, CA, USA). The results are expressed as the mean + standard error of the mean (SEM). Statistical analyses were performed using GraphPad Prism version 8.4.2 (GraphPad Prism, La Jolla, CA, USA). Statistical differences were calculated using a two-tailed unpaired *t*-test. Differences were considered significant when $p < 0.05$, $p < 0.01$, $p < 0.001$.

3. Results

3.1. Fabrication, purification, and storage of MMPsomes

Fig. 2 presents the general approach of MMPsomes fabrication, purification, and storage. For the establishment of MMPsomes, we used the previously described pH-responsive and photo-crosslinked Psomes [31,47,48], with key characteristics: pH, shear-force and storage-stable polymeric vesicles [47,49,50]. MMP-1 molecules were integrated into the membrane of the Psomes using our recently established protein post-loading approach [50]. Validation of the particle shape, membrane conformation and structural parameters (*e.g.*, scaling parameter and apparent density) of post-loaded Psomes was performed by asymmetric flow field-flow fractionation (AF4) coupled to light scattering – an analytical approach established for the detailed characterization of (biologically-active) particles and supramolecular structures [50–53]. This characterization allows to estimate the preferential locations of proteins in/on Psomes – either attached on Psomes surface and/or integrated in Psomes membrane [50]. The knowledge on stability, drug loading efficiency and enzymatic activity after storage is a fundamental requirement for their biomedical application. Thus, thorough physico-chemical characterization of the loaded MMPsomes under relevant storage conditions was performed.

Following fabrication, first experimental steps were focused on the optimization of the purification of fabricated MMPsomes. The loading efficiency of MMP-1 in MMPsomes was estimated using fluorescence spectroscopy. MMP-1 labeled with Rhodamine B (MMP-1-RhB) was used for the subsequent post-loading of swollen Psomes at pH 6.0, at which the intramembrane compartments are accessible for protein loading (Fig. 2A). The concentration of the MMPsomes used in the study was prepared from 0.5 mg BCP/mL and 0.1 mg/mL MMP-1 or MMP-1-RhB. RhB-labeled MMPsomes were purified either by Hollow Fiber Filtration (HFF, MWCO 500 kDa) or dialysis (MWCO 1000 kDa) with 1 mM PBS.

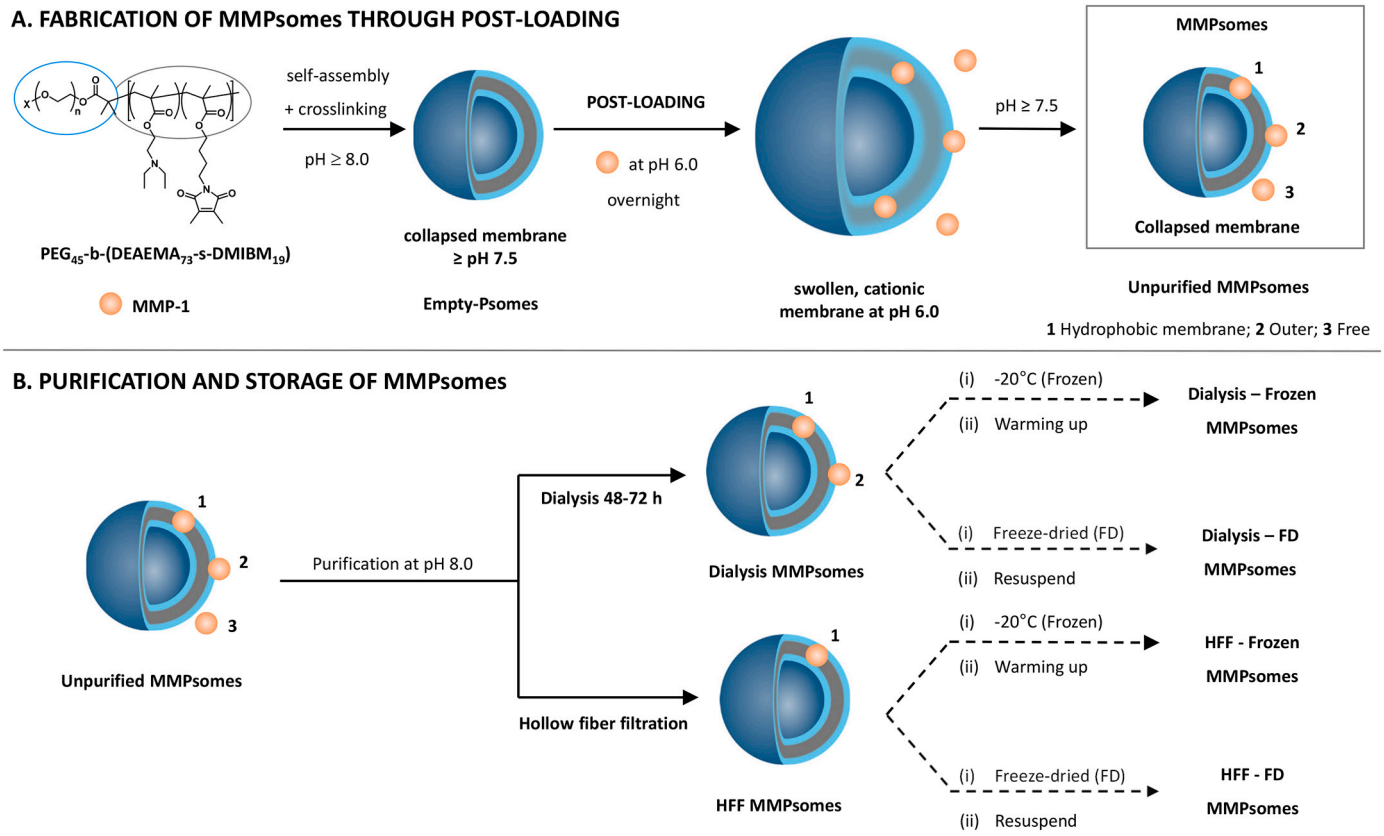

Fig. 2. Schematic representation depicting fabrication, purification, and storage of MMPsomes. A) Formation of MMPsomes through post-loading. Conditions: 0.5 mg BCP/mL + 0.1 mg/mL MMP-1. Schematic representation of postulated MMP-1 localization. B) Purification of MMPsomes at pH 8.0 either using dialysis (48–72 h) or Hollow Fiber Filtration (HFF). Storage was carried out either at −20 °C (frozen) or freeze-dried (FD) in presence of inulin followed by thawing (warming-up) or redispersion, respectively.

After 72 h of dialysis, a high loading efficiency (22%) of MMP-1 in MMPsomes was obtained while only 8% loading efficiency was achieved after HFF purification (Fig. 3A). These differences indicated that depending on the purification procedure, MMP-1 confined at different locations can be removed from the Psomes (as further confirmed by AF4). Obviously under shear-force driven HFF purification, (partially) membrane-integrated MMP-1 in MMPsomes are preferentially present (Fig. 2B, location 1). Finally, a library of MMPsomes (Fig. 2B): unpurified, Dialysis (dialysis-purified), HFF (HFF-purified), Dialysis-Frozen (dialysis-purified and frozen at −20 °C), Dialysis-FD (dialysis-purified and freeze-dried in presence of 0.1 wt% inulin), HFF-Frozen (HFF-purified and frozen at −20 °C) and HFF-FD (HFF-purified and freeze-dried in presence of 0.1 wt% inulin) was used to compare the influence of dialysis and HFF on the solution properties, storage-dependent enzymatic activity (Fig. 3B) and structural parameters (Fig. 4).

3.2. *Analysis of colloidal stability and enzymatic activity of MMPsomes*

We further characterized MMPsomes for the key characteristics such as colloidal stability, pH responsiveness, size, and conformation. The first experimental series was carried out to examine the colloidal stability (R_h) of Empty-Psomes and MMPsomes after purification and storage steps using batch DLS (Table S2). For most samples, R_h were in the range between 42 and 49 nm with polydispersity index (PDI) below 0.22. Contrary, FD samples (Dialysis-FD and HFF-FD) possessed R_h in the range of 63–66 nm with PDI ≥ 0.36. The influence of Dialysis and HFF purification on R_h (43 nm) and PDI (0.21) for unpurified MMPsomes sample was clearly visible, showing lower PDI (≤ 0.15) and similar R_h (42–45 nm). This implies that both purification methods are suitable for removing free unbound MMP-1 from the MMPsomes (Fig. 2A, location 3) without causing particle aggregation. Contrarily, storage of the samples *i.e.*, Dialysis-Frozen, Dialysis-FD, HFF-Frozen, and HFF-FD, led to a general increase in the PDI of samples (Table S2). Furthermore, the freeze-drying process resulted in larger R_h and PDI values, since in that process solid MMPsomes were obtained that upon redispersion in aqueous solution resulted in partially aggregated MMPsomes. It is noteworthy that the freeze-drying process also resulted in a deformation of MMPsomes in the dry state. This can also lead to the break of non-covalent interactions (*e.g.*, ionic interactions and H-bonds) between MMP-1 and Psomes, when "HFF-FD" MMPsomes samples are redispersed afterwards. Overall, these assumptions explain the increase in R_h and PDI values for freeze-dried samples. Summarizing the colloidal stability of purified and stored MMPsomes, most samples were redispersed and were stable in aqueous solution, while Dialysis-FD and HFF-FD showed aggregation upon re-dispersion after storage.

The pH responsiveness of MMPsomes was examined as an additional evidence for the colloidal stability, pH of unpurified Empty-Psomes and MMPsomes solutions were repeatedly switched from pH 9 (collapsed membrane) to 5 (swollen membrane) and analyzed by DLS (Fig. S1). Empty-Psomes and MMPsomes remained stable during at least five swelling-shrinking cycles. This implies no negative effect of MMP-1 on pH-responsiveness of MMPsomes. However, MMPsomes outlined lower swelling ratios compared to Empty-Psomes. It can be assumed that the proteins interacting with the membrane by non-covalent bonds reduce the swelling capacity in MMPsomes. "Dialysis MMPsomes" evidenced similar swelling and collapsing properties and pH* (critical pH at which the turning point between the swollen and shrunken state occurs)[54] as Empty-Psomes (Fig. S2A) when pH-dependent DLS titration in 1 mM PBS was performed. However, aggregates were preferentially generated in presence of the enzyme assay buffer that did not allow the

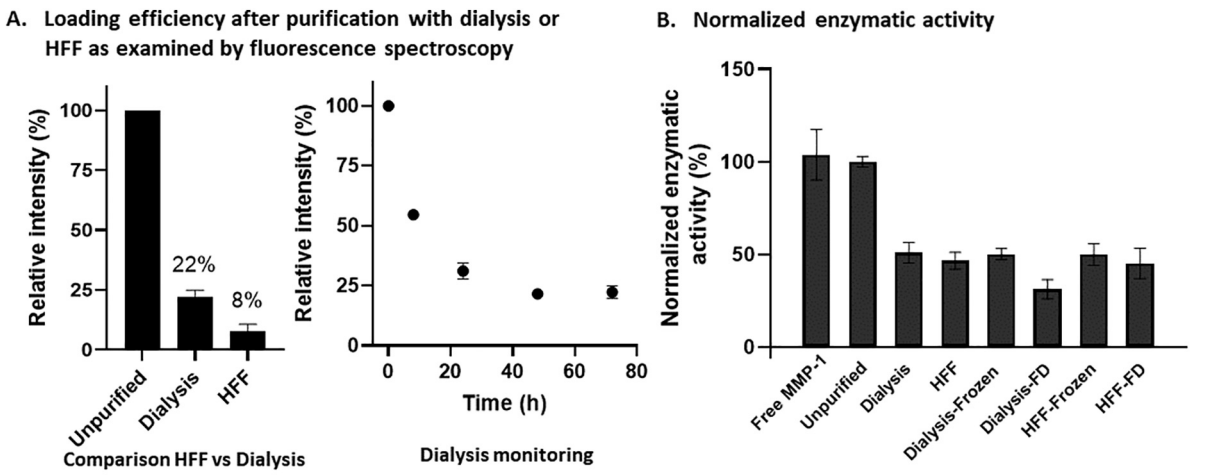

C. Diameter and membrane thickness of crosslinked Psomes studied by cryo-TEM

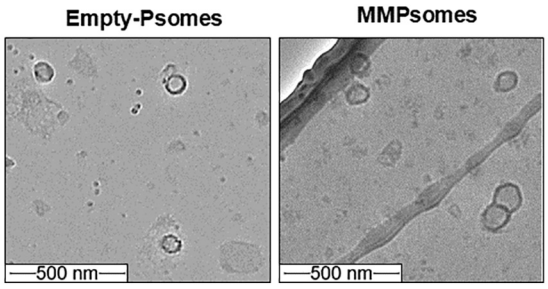

	Empty-Psomes	MMPsomes
Diameter (nm)	86.7 ± 14.0	95.2 + 17.8
Membrane thickness (nm)	15.5 ± 2.5	16.9 ± 1.6
Zeta potential*	16.97 ± 2.05	5.53 ± 3.90

Fig. 3. Characterization of unpurified, dialysis-purified, and HFF-purified MMPsomes for MMP-1 loading efficiency and enzymatic activity, and physicochemical properties (diameter, membrane thickness and Zeta potential). A) Left. Loading efficiency of "Dialysis" and "HFF" MMPsomes by fluorescence spectroscopy (MMP-1-RhB, $\lambda_{ex} = 559$ nm). Right. Loading efficiency of "Dialysis MMPsomes" ($C_{BCP} = 0.25$ mg/mL, $\lambda_{ex} = 559$ nm) over time. The experiments were carried out in triplicate. B) Normalized enzymatic activity of various MMPsomes samples (normalized with 0.1 mg/mL free MMP-1). Normalization was carried out (for each loading approach independently) with "Unpurified MMPsomes" as a reference. Every measurement was carried out in triplicate. C) Cryo-TEM analysis of Empty-Psomes and MMPsomes at pH 8. Diameter, membrane thickness and zeta potential (*mV) of Empty-Psomes and MMPsomes at pH 5 are presented in the table.

determination of membrane properties of MMPsomes (Fig. S2B). Nevertheless, the pH* value for MMPsomes was found to be 6.44 in 1 mM PBS (Fig. S2A), while the collapsing point was around pH 7 (Fig. S2A). Thus, a collapsed MMPsomes membrane can be assumed for all MMPsomes samples during the enzymatic assay (at pH 7.5).

We further analyzed the enzymatic activity of all MMPsomes whereby the enzymatic activities were normalized with the activity of "Unpurified MMPsomes" used as reference (Fig. 3B). In general, all MMPsomes exhibited a measurable and significant enzymatic activity (Fig. 3B) after defined purification and storage protocols. For Dialysis- and HFF-purified MMPsomes, a significant decrease in the MMP-1 enzymatic activity around 50% was observed compared to "Unpurified MMPsomes". In addition, both storage methods (Frozen and FD) maintained an acceptable enzymatic activity: the enzymatic activities after storage were similar or only a bit lower than found for purified MMPsomes before storage. Furthermore, the "Frozen" storage method was found to lead to higher activities than the "FD".

To confirm the previous DLS results, cryo-TEM was performed. Images from the cryo-TEM are presented in Fig. 3C. The diameter of MMPsomes (⌀ ~95 nm) was slightly increased compared to Empty-Psomes (⌀ ~ 87 nm), while a marginal difference in the membrane thickness of about 1–1.5 nm was observed. The results imply that the interactions between MMP-1 and Psomes through the acidic post-loading approach (Fig. 2) result in an enlargement of MMPsomes diameter. This suggests that MMP-1 must be partially integrated in the membrane of Psomes. This membrane integration of MMP-1 also resulted in a very slight increase in membrane thickness. Furthermore, zeta potential (ζ) of free MMP-1 enzyme (isoelectric point = 5.35–6.20) and Empty-Psomes showed an opposite charge density at pH 5 (−5.44 ± 0.84 MMP-1 *versus* 16.97 ± 2.05 Empty-Psomes). MMPsomes displayed a lower ζ (5.53 ± 3.90) compared to Empty-Psomes at pH 5. The ζ results undoubtedly indicate that electrostatic interactions are involved in the formation of MMPsomes (Table S3) at which MMP-1 occupies *per se* the locations 1 and 2 (Fig. 2). MMP-1 locations in MMPsomes ("unpurified", "Dialysis" *etc.*) were further verified by different experiments presented below.

To understand if the post-loading process allow the MMP-1 permeation of swollen Psomes membrane from outside into the lumen at pH 6, we examined whether the substrate (hexapeptide FALGPA) for MMP-1 enzyme assay can cross the MMPsomes membrane, then feeding hypothetically encapsulated MMP-1 in MMPsomes lumen (Fig. 2). Thus, clarification of both scenarios is needed to better understand the enzymatic activity of "Unpurified MMPsomes" sample. To study the membrane diffusion of the substrate, hexapeptide FALGPA, towards MMPsomes at pH 6, 7, and 8, FRET experiments with pH-stable avidin-loaded Psomes and biotinylated peptide were performed under relevant enzymatic buffer conditions (Fig. S3).

At pH 6, biotinylated hexapeptide FALGPA smoothly crossed Psomes membrane for avidin-biotin interactions in the Psomes lumen, while at pH 7 and pH 8, surface attachment and membrane integration of the peptide FALGPA on Psomes can be postulated (Fig. S3). Thus, we concluded that the MMP-1 in the MMPsomes is primarily attached on the surface and partially integrated in the Psomes membrane, but fully accessible to the hexapeptide FALGPA in the enzyme assay. Moreover, it can be assumed that no MMP-1 is localized in the lumen of the MMPsomes.

Since the embedded enzymes might have different accessibility to collagen matrix as compared to FALGPA oligopeptide, we examined the

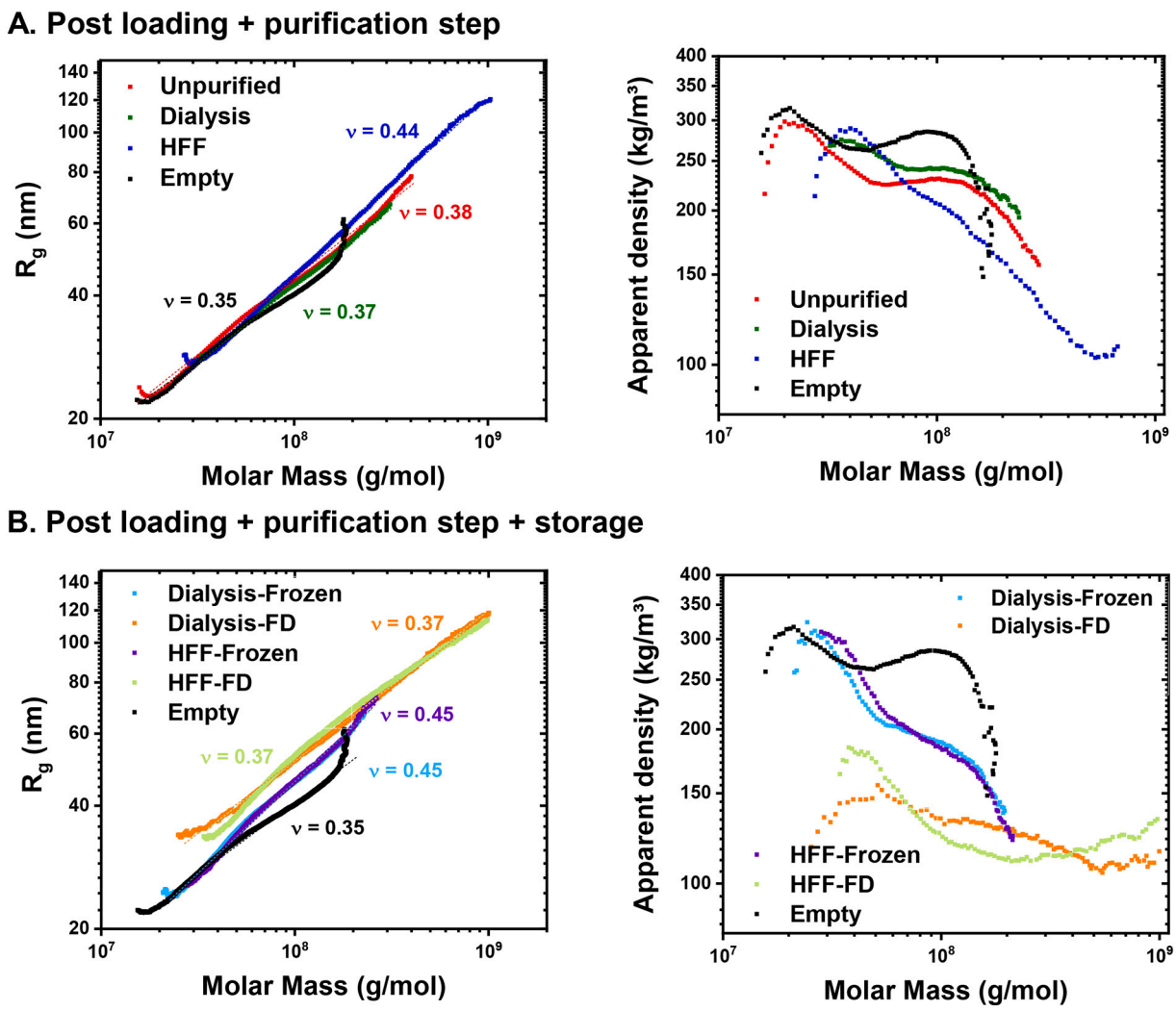

Fig. 4. Conformation plots of Empty-Psomes and MMPsomes measured at pH 8 by AF4-LS. Conditions: 0.5 mg BCP/mL + 0.1 mg/mL MMP-1-RhB. A) Radius of gyration (R_g) (left) and apparent density (right) were calculated for Empty-Psomes, unpurified and purified MMPsomes, and B) Empty-Psomes and purified MMPsomes after storage.

accessibility of MMPsomes (and MMP-1) to 3D collagen matrix. We performed collagen degradation assay where 3D collagen gels were incubated with MMP-1 and MMPsomes. The assay was aligned with the biological assays where human HSCs, LX2 cells, were used. Briefly, human LX2 cells were embedded in the 3D collagen gels and were incubated with equivalent concentrations (1.0 μg/mL) of MMP-1 and MMPsomes, and gel degradation after 48 h of incubation was examined. We observed increased collagen matrix degradation after 48 h of incubation with MMP-1 and MMPsomes as compared to control (no treatment). No significant changes were observed between MMP-1 and MMPsomes suggesting that MMPsomes have more or less equal accessibility to the collagen matrix as free MMP-1 (Fig. S4).

3.3. *Characterization of MMPsomes by asymmetric flow field-flow fractionation (AF4)*

The consequences of each purification and storage process on the conformation and size of the MMPsomes were estimated after characterization with AF4 combined with static light scattering (SLS) or dynamic light scattering (DLS) (Fig. 4). To obtain more reliable results about the molecular characteristics of MMPsomes, and to separate and analyze particles with different sizes discretely, the coupling of AF4 with light scattering technique (AF4-LS) was used [50–53]. The molar mass and radii of gyration (R_g) distributions of the different samples were determined, and a conformation plot R_g *vs* M_w provided valuable information on the compactness of the Psomes, based on the theory of the scaling law, thus, unlocking the preferential location of the proteins [50]. The summarized results of AF4 measurements of Empty-Psomes and different MMPsomes and free MMP-1 quantification in MMPsomes after AF4 separation have been provided in Tables S4 and S5.

Fig. 4A-B shows the conformation behaviour of Empty-Psomes, purified and unpurified MMPsomes before and after storage. Empty-Psomes possess scaling exponent (ν) of 0.35 that is close to the theoretical value of perfectly spherical object (0.33). Yet, post-loading of Psomes with MMP-1 (Unpurified, Dialysis and HFF) leads to a slight increase from 0.37 for Unpurified to 0.38 for Dialysis, and 0.44 for HFF MMPsomes (Fig. 4A). The apparent density of MMPsomes (Unpurified, Dialysis and HFF) *versus* Empty-Psomes (Fig. 4A) showed a similar behaviour as the scaling parameter. However, the slight decrease of the apparent density of MMPsomes may prove the incorporation of the MMP-1 into the Psomes membrane. Yet, "HFF MMPsomes" showed the highest decrease in density compared to the other MMPsomes. In addition, an increased dispersity for "HFF MMPsomes" was also observed due to aggregation, as shown by an increase in the molar mass.

The effect of the storage conditions – Frozen or FD – was also analyzed in detail using AF4-LS. The conformation plots in Fig. 4B

demonstrated the same scaling exponent of 0.45 for the "Frozen MMPsomes" samples independent of the purification procedure. The same scaling parameter ($\nu = 0.37$) was also observed for both "FD MMPsomes" samples which is close to "Empty-Psomes" sample ($\nu = 0.35$). Both "Dialysis-FD" and "HFF-FD" outlined the lowest apparent density compared to "Frozen MMPsomes" and reference "Empty-Psomes" (Fig. 4B). Here again, "FD MMPsomes" indicated the presence of larger molar masses due to slight aggregation of FD MMPsomes in solution. This is in accordance with the results of batch DLS despite the existence of even more compact vesicular structures of "Dialysis-FD" and "HFF-FD" when comparing only their ν values with reference "Empty-Psomes" (Fig. 4B).

3.4. Selection and in-depth characterization of MMPsomes

Based on the previous characterization of all MMPsomes, we selected "Dialysis MMPsomes" for the biological studies due to their stable solution properties (Table S2), molecular parameters (Fig. 4), high loading efficiency (Fig. 3A), as well as their favorable enzymatic activity after storage (Fig. 3B).

"Dialysis MMPsomes" were prepared with a high concentration of MMP-1 (0.5 mg BCP/mL and 0.2 mg MMP-1/mL) as required for further biological experiments, and under these conditions, loading efficiency (Fig. S4) and storage stability were verified again. A high loading efficiency was established after dialysis of MMPsomes after 48 h (Fig. S5). These "Dialysis MMPsomes" also provided sufficient storage stability at 4 °C for 7 days and MMP-1 still showed high enzymatic activity in enzyme assay for MMP-1 after 7 days (91%) compared to 1 day (100%) (Fig. S6). To prepare fresh or 4 °C stored "Dialysis MMPsomes", Empty-Psomes aliquots can be stored at −20 °C for several weeks. Thus, storage stability, membrane properties, pH sensitivity and enzymatic activity of "Dialysis MMPsomes" were found to be suited for the biological experiments.

Moreover, we performed stability studies of Empty-Psomes and Dialysis MMPsomes in 1 mM PBS, 10% FBS in 1 mM PBS and serum-free medium. Briefly, Dialysis MMPsomes ($C_{Empty\text{-}Psomes} = 0.25$ mg BCP/mL and $C_{MMP\text{-}1} = 0.1$ mg/mL), and Empty-Psomes ($C_{Empty\text{-}Psomes} = 0.25$ mg BCP/mL) were incubated at 37 °C in three different solutions: a) 1 mM PBS, b) 10% FBS in 1 mM PBS and c) serum-free DMEM medium. All samples were analyzed by DLS after different time points of incubation (0, 2, 4, 6, 8, 24 and 48 h). The results are shown in the Tables S6 and S7. Empty-Psomes possess a high colloidal stability under all selected conditions up to 48 h, except in 10% FBS in 1 mM PBS up to 8 h. In contrast, Dialysis MMPsomes showed a time-dependent colloidal stability for the first 8 h in 10% FBS in 1 mM PBS, then aggregation processes can be observed between 8 and 24 h, while in both other solutions a preferred colloidal stability can be assumed. The results also confirm that Dialysis MMPsomes will be stable for a longer period over hours and days, depending on the biological fluids. It should be noted that both Empty-Psomes and MMPsomes exhibited favorable colloidal stability in serum-free medium in which all the biological experiments are performed.

We further performed the MMP-1 release experiment after short-term cyclic protonation and deprotonation steps in the membrane of MMPsomes. Results, as presented in Fig. S7, suggest that MMP-1 provides high non-covalent interactions with the membrane of MMPsomes. Despite the (cyclic) short-term swelling process, most of the MMP-1 biomacromolecules were preferentially entrapped in the membrane. This observation also supports the working hypothesis of membrane-integrated MMP-1 in MMPsomes validated by cryo-TEM and other characterization methods in this study.

3.5. Effect of MMP-1 on TGFβ-induced collagen I expression in human HSCs

Before performing experiments with MMPsomes, the appropriate therapeutic concentration of MMP-1 should be established. Therefore, experiments with different concentrations of MMP-1 (0.5–5.0 μg/mL) were performed on transforming growth factor beta (TGFβ)-activated human HSCs (LX2 cells), the key pathogenic cells producing large amounts of col-I, the major ECM protein. TGFβ has shown to induce a myofibroblast-like migratory phenotype in human HSCs with high col-I expression [55,56]. The effect of different concentrations of MMP-1 was examined on the col-I expression at mRNA and protein level using quantitative real-time PCR and western-blot (WB) respectively (Fig. 5A-C). We found high upregulation of col-I mRNA ($p < 0.05$) and protein ($p < 0.001$) expression induced by TGFβ and a dose-dependent inhibition by MMP-1. The lowest concentration (0.5 μg/mL) showed some inhibition in col-I protein expression, however non-significant, while the highest two concentrations (1.0 and 5.0 μg/mL) showed significant inhibition ($p > 0.05$) (Fig. 5A,B). At the mRNA level, there was a dose-dependent inhibition in *col1a1* gene expression, with increasing significance upon MMP-1 treatment (Fig. 5C).

3.6. Effects of MMP-1 on MMP-1/TIMP-1 ratio and TGFβ-induced migration of human HSCs

MMP-1 and TIMP-1 expression in fibrotic livers are imbalanced with reduced MMP-1 expression and increased TIMP-1 expression [8,57]. This imbalance can be measured with the MMP-1/TIMP-1 ratio using PCR. We examined this ratio and found it is significantly decreased upon TGFβ activation ($^{*}p < 0.05$), while this ratio was dose-dependently increased by MMP-1 treatment, with significant results in the highest two concentrations (1.0 and 5.0 μg/mL) (Fig. 5D).

Besides excessive ECM production, activated HSC are highly migratory and migrate towards the site of injury [58,59]. The migration of non-stimulated, TGFβ-stimulated and MMP-1 + TGFβ treated HSCs was assessed using a standardized scratch/wound healing assay. Aligned with the previous results, the migration of the TGFβ-activated cells was significantly increased after 24 h ($^{**}p < 0.01$), as shown in Fig. 5E. Furthermore, a dose-dependent and significant inhibition of TGFβ-induced HSCs migration by MMP-1 treatment was evidenced (Fig. 5E). The therapeutic effects can be influenced by cell viability therefore the effect of different concentrations of MMP-1 on the viability of LX2 cells was examined using Alamar blue assay. Expectedly, no effect of MMP-1 on the cell viability was observed (Fig. 5F).

3.7. Evaluation of the therapeutic effects of MMPsomes on TGFβ-activated human HSCs (LX2) in vitro

Based on the previous experiments (Fig. 5), an effective MMP-1 concentration *i.e.*, 1.0 μg/mL was selected for evaluating the therapeutic effects of MMPsomes. In the following experiments, cells were treated with medium alone, TGFβ (5 ng/mL) ± MMP-1 (1.0 μg/mL), Empty-Psomes (Psomes, 4.17 μg/mL equivalent to MMPsomes), MMP-1 (1.0 μg/mL) + Empty-Psomes (Psomes, 4.17 μg/mL equivalent to MMPsomes) (MMP-1 + Psomes), and MMPsomes (1.0 μg/mL MMP-1 and 4.17 μg/mL Psomes).

The treatment effects of MMPsomes were first examined on protein and gene expression of col-I using western blot and ELISA, and quantitative PCR respectively (Fig. 6A-C, and Fig. S8). In general, MMPsomes evidenced higher inhibition in col-I expression compared to free MMP-1, MMP-1 + Psomes and Psomes. At the protein level, MMPsomes showed increased therapeutic efficacy with highest significance (Fig. 6A-B, and Fig. S8), while MMP-1 alone or co-incubated with Psomes (MMP-1 + Psomes) showed some inhibitory effects. Likewise, at the gene expression level, no effect of the Psomes and MMP-1 + Psomes was observed, in contrast to free MMP-1 ($^{*}p < 0.05$) and MMPsomes ($^{**}p < 0.01$), where both MMP-1 and MMPsomes showed significant inhibition in col-I expression (Fig. 6C). Furthermore, the MMP-1/TIMP-1 ratio was decreased in TGFβ-activated LX-2 cells and was significantly by increased MMPsomes ($^{***}P < 0.001$) treatment, while no significant increase upon Psomes, MMP-1 and MMP-1 + Psomes treatment was

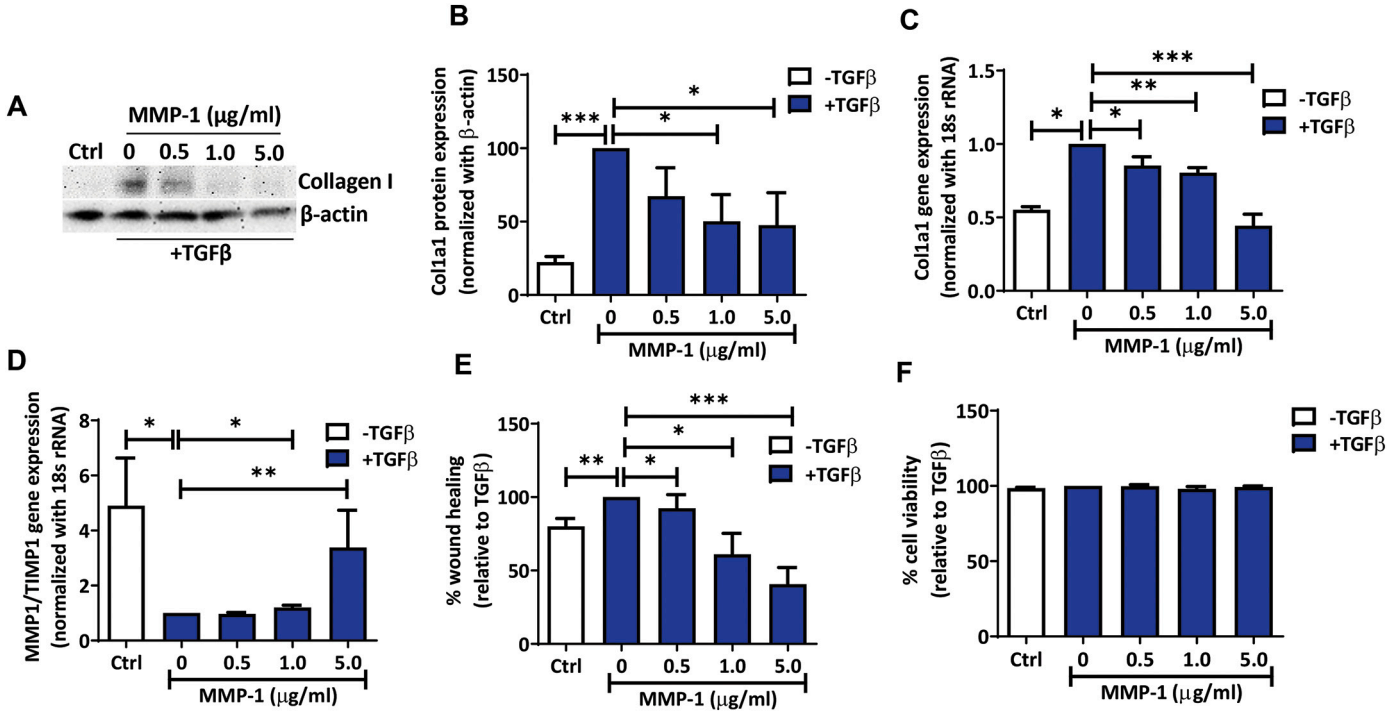

Fig. 5. Effect of different concentrations of MMP-1 on TGFβ-activated human HSCs. A) Representative western blot images and B) Quantified col-I protein expression (normalized to β-actin) after 48 h of treatment; C) Col-1a1 and D) MMP-1/TIMP-1 gene expression (normalized to 18 s rRNA); E) Relative wound healing (%) and F) Cell viability (%), relative to TGFβ (at 100%), after 24 h of treatment with medium (Ctrl) and TGFβ with different concentrations of MMP-1. Results are presented as mean + SEM of at least three independent experiments. $^{*}p < 0.05$; $^{**}p < 0.01$ and $^{***}p < 0.001$.

observed (Fig. 6D). Lastly, MMP-1, MMP-1 + Psomes, and more significantly MMPsomes treatment resulted in reduced migration (wound healing response) of LX2 cells (Fig. 6E). Effect of MMPsomes on cell viability was also examined and found that 1.0 μg/mL MMPsomes (and MMP-1 + Psomes) showed improvement in cell viability (> 80% cell viability) as compared to Psomes (~72% cell viability) (Fig. 6F).

3.8. MMPsomes ameliorated fibrosis and inflammation in the CCl_4-induced early liver fibrosis model in vivo

Subsequently, the therapeutic effects of MMPsomes *versus* MMP-1 were evaluated *in vivo* in a carbon-tetrachloride (CCl_4)-induced early liver fibrosis mouse model (Fig. 7A). Empty-Psomes did not show any significant effects in the *in vitro* studies therefore were excluded from the *in vivo* studies, to reduce the number of animals, further supported by a previous study where no effects of Empty-Psomes was observed *in vivo* [60]. To evaluate MMP-1 and MMPsomes *in vivo*, a single intraperitoneal injection of CCl_4 (at day 1) was administered to induce early liver fibrosis followed by a single intravenous injection of PBS, MMP-1 (10 μg/mice/dose) or MMPsomes (10 μg MMP-1 with 41.7 μg Psomes/mice/dose) (at day 3). At day 4, all the animals were sacrificed, and livers were harvested for further analysis. Increased liver weight and liver/body weight ratio ($^{***}p < 0.001$) was evidenced in CCl_4 mice as compared to control healthy mice as also reported previously [61] (Fig. 7B), associated with increased col-I (an ECM marker, indicative of fibrosis) [55] and F4/80 expression (a macrophage marker, indicative of inflammation) [62] (Fig. 7C). The liver weights and liver/body weight ratio decreased significantly upon MMPsomes treatment, while free MMP-1 showed no significant effect (Fig. 7C). Furthermore, MMPsomes attenuated col-I and F4/80 expression suggesting amelioration of early fibrosis and inflammation respectively after MMPsomes treatment as compared to MMP-1 treatment (Fig. 7C). Recently, it has been demonstrated that activated fibroblasts generate deformation fields in fibrillar collagen matrix that provide far-reaching physical cues to attract and guide macrophages [63]. We postulate that collagen degradation resulted in the loss of these mechanical cues and therefore resulted in reduction of macrophage chemotaxis thus liver inflammation. These results suggest that MMPsomes efficiently attenuates early liver fibrosis by degrading collagen-rich matrix and macrophage infiltration.

4. Discussion

Liver fibrosis, a life-threatening disease affecting millions of people world-wide, is not yet curable [6]. The excessive deposition of col-I resulting in progressive fibrosis is mainly caused by activated HSCs (liver fibroblasts), the major cellular targets in the search for therapeutic agents in liver fibrosis [57]. Pathological remodeling of ECM by fibroblasts plays a key role in organ failure. More importantly, aberrant diseased ECM has been proposed to be the predominant driver that drives the fibrosis progression [64]. In this study, we proposed collagen type-I degrading MMPsomes (MMP-1-decorated polymersomes), a novel surface-active extracellular matrix therapeutic, as a promising approach for the treatment of liver fibrosis. We successfully developed biologically active MMPsomes that were extensively characterized for favorable physicochemical properties, MMP-1 loading efficiency, storage stability and enzymatic activity. MMPsomes were evaluated for their therapeutic effectiveness *in vitro* on TGFβ-activated HSCs and *in vivo* in early fibrosis mouse model, whereby MMPsomes showed improved therapeutic effects as compared to free MMP-1 in inhibiting liver fibrosis.

For a development of biologically-active MMPsomes, the following key characteristics are essential: pH, osmotic and shear-force stability between pH 6.0 and 8.0 where non-covalent interactions between MMP-1 and Psomes are the driving forces to adhere MMP-1 at the outer membrane surface of Psomes. High stability of MMPsomes is required for the fabrication, purification (dialysis and shear-force driven HFF), and storage (Fig. 3). Furthermore, MMPsomes should possess a necessary enzymatic activity after the fabrication, purification and storage steps (Fig. 4). Especially, the enzymatic storage stability of MMPsomes is

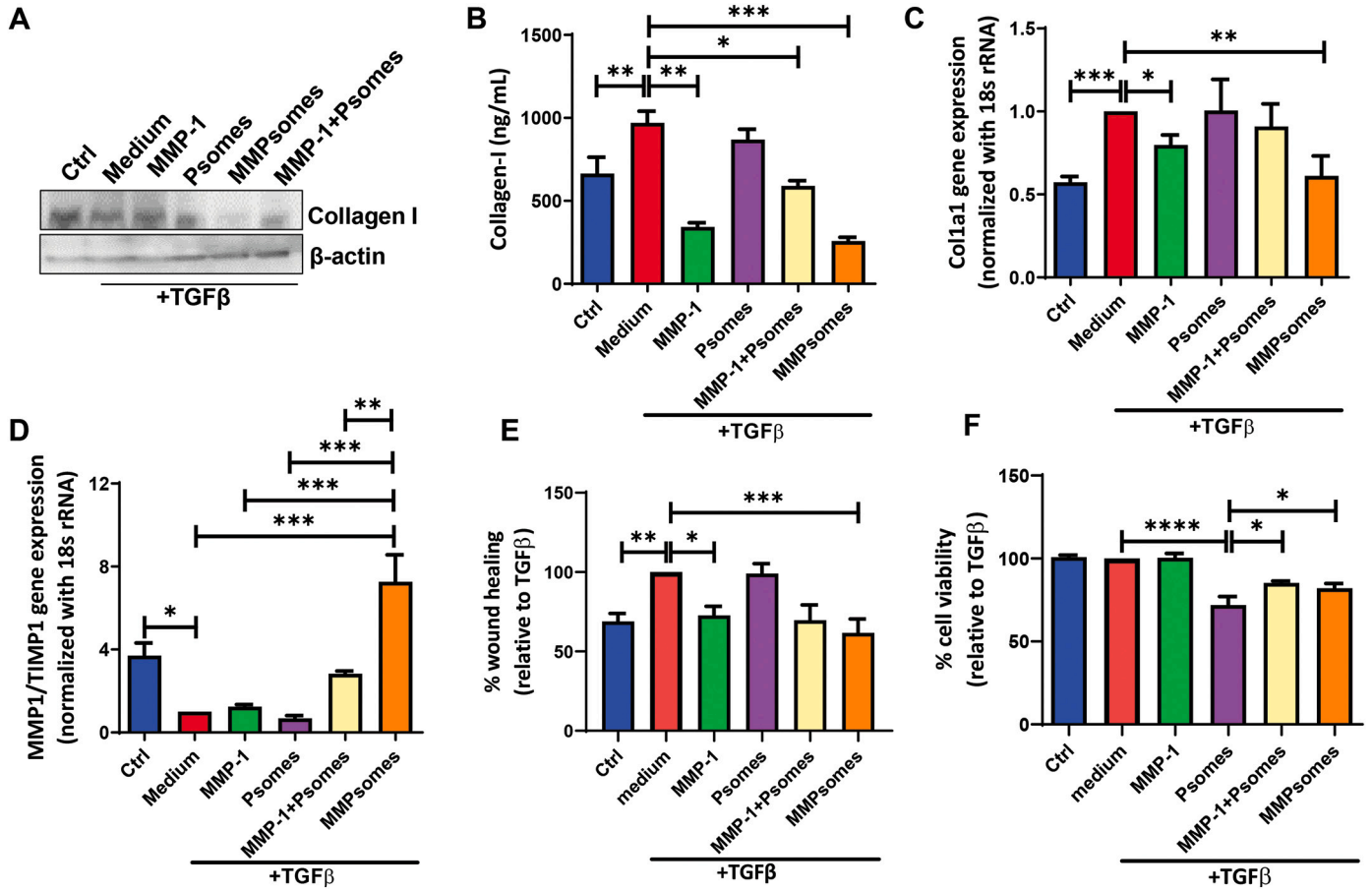

Fig. 6. Effects of MMPsomes on TGFβ-activated human HSCs. A) Representative western blot images (refer to Fig. S8 for quantitative analysis) and B) Total Col-I expression in culture supernatant as assessed using ELISA after 48 h treatment; C) Col-I and D) MMP-1 and TIMP-1 gene expression normalized to 18 s rRNA; E) Relative wound healing (%) and F) Cell viability (%), relative to TGFβ (at 100%), after 24 h of treatment with control medium (Ctrl) and 5 ng/mL TGFβ ±1.0 μg/mL MMP-1, Psomes, MMP-1 + Psomes or MMPsomes. Results are presented as mean + SEM of at least three independent experiments. *$p < 0.05$; **$p < 0.01$; ***$p < 0.001$ and ****$p < 0.0001$.

one deciding requirement for their final biological action in our study (Figs. 5, 6, 7). Finally, MMPsomes should be biocompatible towards different cells and extracellular matrix, but also more efficient compared to free MMP-1 in biological functions.

As confirmed from the fabrication and characterization results, MMPsomes showed the desired characteristics (*e.g.* pH-, osmotic- and shear-force-stability). Especially, MMPsomes were still enzymatically active after been stored for short-term (1–3 days at 4 °C or − 20 °C) or long-term (7 days at 4 °C) periods. Moreover, Empty-Psomes frozen at −20 °C could be shipped/and used for the preparation of MMPsomes by the MMP-1 post-loading, followed by different purification and storage processes (*e.g.* "fresh Dialysis MMPsomes" and "Dialysis-4 °C stored MMPsomes" samples). The simplicity of the post-loading process for preparing different MMPsomes samples is remarkable, and the colloidal stability of Psomes and MMPsomes after their storage at different low temperatures (from −20 °C to 10 °C) to fabricate pH- and shear-force-stable MMPsomes ("Dialysis", "HFF", "Dialysis-Frozen" and "HFF-Frozen") for the biological experiments. Freeze-dried MMPsomes ("Dialysis-FD" and "HFF-FD") outlined a low degree of undesired aggregation properties after re-dispersion process. This extensive study on the purification, storage and solution properties of MMPsomes undoubtedly confirms preliminary results on the storage and solution behaviour of pH-responsive Psomes with *in situ* loaded myoglobin and surface modified with HSA protein [49,50].

Importantly, independent of the purification step, dialysis and HFF, most MMPsomes displayed similar enzymatic activities (Fig. 3B). This is surprising, since a lower post-loading efficiency for MMP-1 (8%) in "HFF samples" compared to the "Dialysis samples" (22%). It is important to consider that the enzymatic assay offers only an estimate of the residual enzymatic activity; a more in-depth study should be carried out to make a quantitative calculation in future, not required for the present investigation.

From cryo-TEM and AF4 studies, it can be postulated that MMP-1 biomacromolecules, partially integrated in the membrane, are responsible for the increase in diameter and membrane thickness (Fig. 3C), and, thus, occupy the location 1 in MMPsomes. The key characteristic of slightly increased membrane thickness for identifying membrane-integrated proteins in Psomes is always combined with increasing, decreasing and similar diameters as confirmed by previously published reports [50,65]. Furthermore, MMP-1 biomacromolecules are also, to some extent, attached on the surface (Fig. 2, location 2). The main non-covalent interactions for MMP-1 in location 2 are ionic interactions and H-bonds, and other physical forces which are preferentially broken under shear-force driven HFF purification postulating preferred location 1 for MMP-1 in "HFF MMPsomes". Moreover, such non-covalent interactions are responsible for the preferred non-releasing properties of MMP-1 from MMPsomes, when exposed to physiological environment and *in vivo*. AF4 study further confirms the different post-loading state of MMP-1 in "Dialysis" and "HFF" MMPsomes samples (Fig. 4A). This does not lead to perfect spherical shapes of MMPsomes as found for "Empty-Psomes", but to less homogeneous conformation and to more open and less smooth Psomes surface in MMPsomes samples, indicated by an increase of the scaling exponent (Fig. 4A). Results of batch DLS (Table S5) are further confirmed by AF4 results. Especially, "HFF MMPsomes"

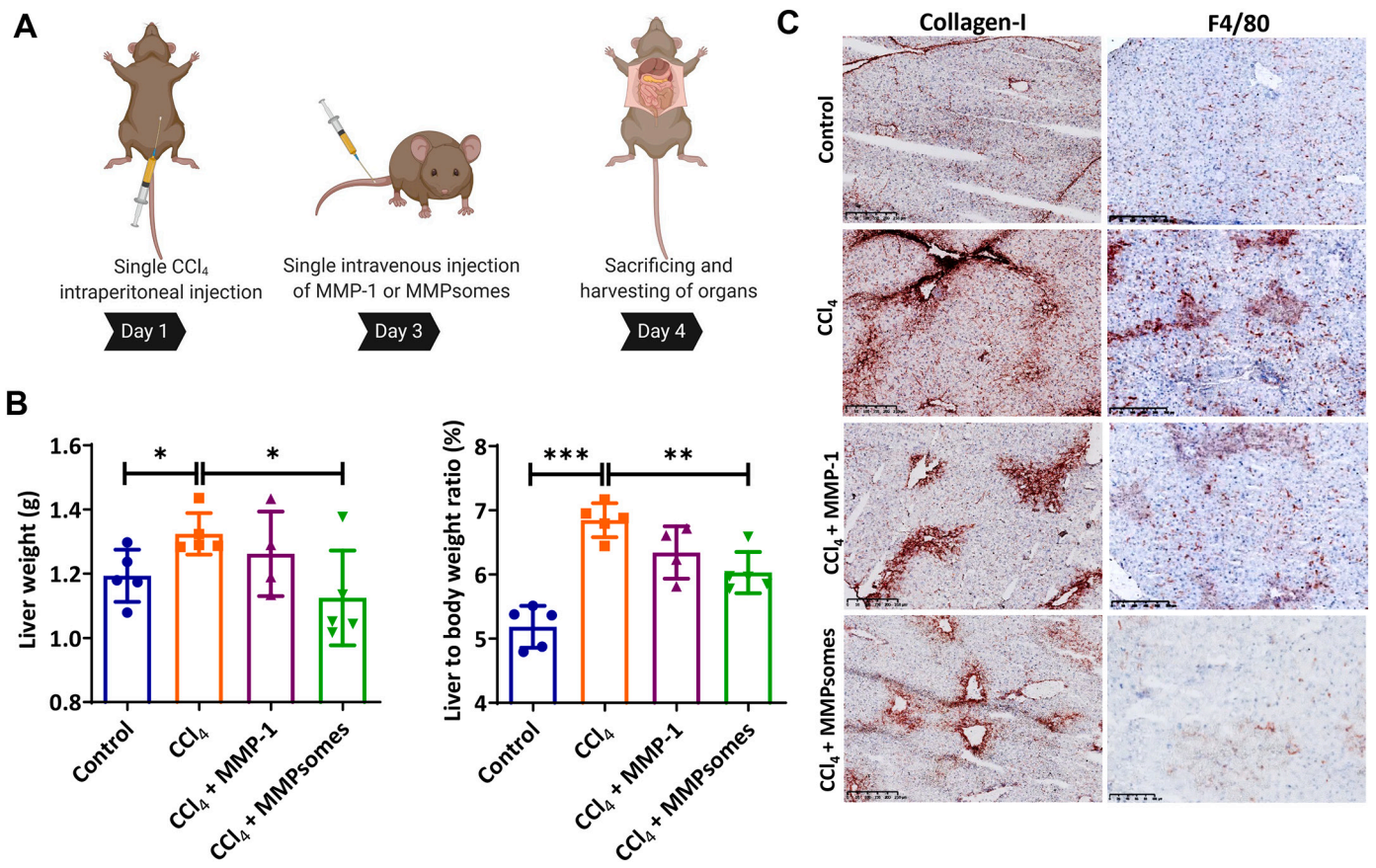

Fig. 7. Effects of MMPsomes in CCl_4-induced early liver fibrosis mouse model. A) Schematic presentation of a timeline of a mouse experiment. After administration of single CCl_4 injection (at day 1), mice received single treatment of MMP-1 and MMPsomes (day 3) intravenously and were sacrificed at day 4. Created with Biorender.com B) graphs showing liver weights (g) and Liver to body weights (%) of healthy mice and CCl_4 with and without treatment with MMP-1 and MMPsomes. C) Representative images of collagen I (ECM marker) and F4/80 (macrophage marker) stained liver sections from control group ($n = 5$), CCl_4 group (CCl_4 mice treated with PBS, n = 5), CCl_4 + MMP-1 group (CCl_4 mice treated with free MMP-1, 10 μg/mice/dose, $n = 4$), and CCl_4 + MMPsomes group (CCl_4 mice treated with MMPsomes, 10 μg/mice/dose, n = 5). Results are presented as mean ± SEM. *$p < 0.05$; **$p < 0.01$ and ***$p < 0.001$.

sample outlined slight aggregation in the conformation plot for larger molar masses, but also "Dialysis-FD" and "HFF-FD" MMPsomes exhibited slight aggregation after their-re-dispersion. Overall, the characterization of all MMPsomes samples outlined that most samples are suited for carrying out biological experiments due to their well-defined solution properties, but depends on particular storage conditions. For simplification to prepare MMPsomes samples for biological study, we decided to use "Dialysis MMPsomes" samples, showing favorable storage properties at 4 °C and, finally, as enzymatically surface-active MMPsomes (Fig. S6).

With successful establishment of enzymatically active MMPsomes, we have been able to study the biological potential of MMPsomes compared to free MMP-1. Firstly, the *in vitro* efficacy of free MMP-1 was evaluated. To mimic the fibrotic liver, we used immortalized hepatic stellate cell line (LX-2) which was activated using TGFβ, inducing transdifferentiation into highly fibrotic migratory col-I producing stellate cells. Efficacy was proven by significant increase in col-I production at mRNA and protein level, accompanied by pathological MMP-1/TIMP-1 ratio and increased wound healing (Fig. 5). As seen in all different aspects of fibrotic phenotype, col-I, MMP-1 and TIMP-1 expression and migration, MMP-1 showed inhibition and stabilization towards healthy phenotype, which in accordance with the literature [18]. These findings support our hypothesis of fibrosis amelioration due to ECM turnover.

To predict the efficacy of MMPsomes *in vivo,* comparative *in vitro* studies were performed between MMP-1 and MMPsomes showing increased efficacy of MMPsomes over free MMP-1 (Fig. 6). As discussed before, MMPsomes provided protection to activity loss due to long-term storage, compared to free MMP-1. In all criteria, col-I protein and mRNA expression, MMP-1/TIMP-1 expression and migration (wound healing response), an improved efficacy of MMPsomes was observed when compared with free MMP-1 (Fig. 6). Interesting is the MMP-1/TIMP-1 ratio, which is significant higher in MMPsomes compared to control and other treatments (Fig. 6D). The high MMP-1/TIMP-1 ratio implicating higher expression of MMP-1 compared to its counterpart TIMP-1 leads to degradation of the col-I rich ECM favoring resolution of fibrosis.

Since the *in vitro* results showed negligible effects of Empty-Psomes, the *in vivo* experiments were performed using free MMP-1 and MMPsomes, to reduce the number of mice. We found that the CCl_4-induced acute fibrosis mouse model showed amelioration of fibrosis with a single dose of 10 μg MMPsomes. The liver-body weight ratio showed significant decrease upon MMPsomes treatment, while the effect of MMP-1 was insignificant, supporting our hypothesis that MMPsomes have higher efficacy. Furthermore, the effect on liver inflammation and fibrosis was analyzed (Fig. 7). F4/80 is an important marker for the persistent inflammation present in fibrosis [55], while col-I, represents the fibrotic ECM [62]. The increase col-I and F4/80 expression found in the fibrotic mouse was strongly reduced upon MMPsomes, compared to free MMP-1, further supporting our hypothesis that the degradation of ECM by enzymatically active MMPsomes is a promising therapeutic in the fight against liver fibrosis.

For future clinical application of Empty-Psomes and/or MMPsomes, it is important to investigate their *in vivo* biodegradability, biocompatibility and clearance. Our Empty-Psomes are composed of the hydrophilic PEG segment, and the hydrophobic part containing pH-sensitive

2-(N,N-diethylamino)ethyl methacrylate (DEAEMA) and a photo-crosslinker 3,4-dimethyl maleic imidobutyl methacrylate (DMIBM). It should be noted that degradation of DEAEMA (and possibly DMIBM) produces non-hydrolysable, but water-soluble, oligomeric and polymeric DMAEMA structures as reported previously [66]. Based on this study, and other supporting studies, we speculate that our Empty-Psomes or MMPsomes will be cleared by the kidney following intravenous administration [67]. More in-depth studies are however warranted in this direction.

In a recent study, Fan and Zhang et al., synthesized a collagenase-I and retinol decorated polymeric micelle (CRM) with nanodrill-like and HSCs-targeting activities, that accumulated in the fibrotic liver and targeted activated HSCs *in vivo* [68]. Moreover, CRM loaded with a tyrosine kinase inhibitor nilotinib (CRM/NIL) evidenced anti-fibrotic effects [68]. The development of ECM penetrating MMP-1/collagenase-I therapeutics, suggested in our (and this recently published) study, offer new horizons for treating liver fibrosis. Their potential can be in the underlying degradation of densified collagen matrix by (surface-active) ECM penetrating MMP-1 therapeutics which, finally, support the self-stimulating and/or self-recovering process. Moreover, our study exhibits an extensive characterization of the protein therapeutics that can be extrapolated to other protein therapeutics, where the post-loading methodology used is simple and versatile.

In conclusion, in this study, we demonstrate shear-force-stable, storable, enzymatically active MMPsomes (MMP-1 decorated polymersomes) with effective amelioration of fibrosis. Post-loading of MMP-1 on stable and pH-responsive Psomes at pH 6, ensuring anchoring of MMP-1 in the membrane or on the outer-membrane surface of Psomes, leading to stable, robust, and enzymatically active MMPsomes. This easily fabricated surface-active ECM-therapeutic preserves enzymatic activity upon long-term storage over several days. In general, this makes MMPsomes suitable for technical use in a reproducible way. The degradation of excessive col-I in the fibrotic ECM by MMPsomes results in the inhibition of fibrotic markers in TGFβ-activated LX-2 cells *in vitro* and CCl_4-induced fibrotic mouse model *in vivo*. Altogether, this study provides an approach for ECM therapeutics to deliver MMP-1 for the degradation of fibrotic ECM, resulting in amelioration of liver fibrosis. This approach may also open new avenues for the delivery of other surface-active ECM protein therapeutics.

Financial support

This study was supported by the University of Twente, and the European Association for the Study of the Liver (EASL).

Acknowledgements

The authors gratefully acknowledge Bettina Pilch for supporting fluorescence spectroscopy and Christina Harnisch for carrying out SEC measurements.

Appendix A. Supplementary data

Supplementary data to this article can be found online at https://doi.org/10.1016/j.jconrel.2021.03.016.

References

[1] D. Schuppan, N.H. Afdhal, Liver cirrhosis, Lancet 371 (2008) 838–851.
[2] C.-Y. Zhang, W.-G. Yuan, P. He, J.-H. Lei, C.-X. Wang, Liver fibrosis and hepatic stellate cells: etiology, pathological hallmarks and therapeutic targets, World J. Gastroenterol. 22 (2016) 10512–10522.
[3] Y.S. Lim, W.R. Kim, The global impact of hepatic fibrosis and end-stage liver disease, Clin. Liver Dis. 12 (2008) 733–746 (vii).
[4] M. Blachier, H. Leleu, M. Peck-Radosavljevic, D.-C. Valla, F. Roudot-Thoraval, The burden of liver disease in Europe: a review of available epidemiological data, J. Hepatol. 58 (2013) 593–608.
[5] Z.M. Younossi, L. Henry, H. Bush, A. Mishra, Clinical and economic burden of nonalcoholic fatty liver disease and nonalcoholic steatohepatitis, Clin. Liver Dis. 22 (2018) 1–10.
[6] R. Bansal, B. Nagórniewicz, J. Prakash, Clinical advancements in the targeted therapies against liver fibrosis, Mediat. Inflamm. 2016 (2016) 7629724.
[7] J. Wiegand, T. Berg, The etiology, diagnosis and prevention of liver cirrhosis: part 1 of a series on liver cirrhosis, Dtsch. Arztebl. Int. 110 (2013) 85–91.
[8] K. Böttcher, M. Pinzani, Pathophysiology of liver fibrosis and the methodological barriers to the development of anti-fibrogenic agents, Adv. Drug Deliv. Rev. 121 (2017) 3–8.
[9] M. Roderfeld, Matrix metalloproteinase functions in hepatic injury and fibrosis, Matrix Biol. 68-69 (2018) 452–462.
[10] S. Duarte, J. Baber, T. Fujii, A.J. Coito, Matrix metalloproteinases in liver injury, repair and fibrosis, Matrix Biol. 44-46 (2015) 147–156.
[11] A. Naim, Q. Pan, M.S. Baig, Matrix Metalloproteinases (MMPs) in liver diseases, J. Clin. Exp. Hepatol. 7 (2017) 367–372.
[12] E. Geervliet, R. Bansal, Matrix metalloproteinases as potential biomarkers and therapeutic targets in liver diseases, Cells 9 (2020) 1212.
[13] J. Gross, C.M. Lapiere, Collagenolytic activity in amphibian tissues: a tissue culture assay, Proc. Natl. Acad. Sci. U. S. A. 48 (1962) 1014–1022.
[14] W. Ando, H. Yokomori, N. Tsutsui, E. Yamanouchi, Y. Suzuki, M. Oda, Y. Inagaki, K. Otori, I. Okazaki, Serum matrix metalloproteinase-1 level represents disease activity as opposed to fibrosis in patients with histologically proven nonalcoholic steatohepatitis, Clin. Mol. Hepatol. 24 (2018) 61–76.
[15] Y. Murawaki, Y. Ikuta, Y. Idobe, H. Kawasaki, Serum matrix metalloproteinase-1 in patients with chronic viral hepatitis, J. Gastroenterol. Hepatol. 14 (1999) 138–145.
[16] G.B. Fields, Interstitial collagen catabolism, J. Biol. Chem. 288 (2013) 8785–8793.
[17] J.L. Lauer-Fields, G.B. Fields, Triple-helical peptide analysis of collagenolytic protease activity, Biol. Chem. 383 (2002) 1095–1105.
[18] Y. Iimuro, T. Nishio, T. Morimoto, T. Nitta, B. Stefanovic, S.K. Choi, D.A. Brenner, Y. Yamaoka, Delivery of matrix metalloproteinase-1 attenuates established liver fibrosis in the rat, Gastroenterology 124 (2003) 445–458.
[19] C. Du, M. Jiang, X. Wei, J. Qin, H. Xu, Y. Wang, Y. Zhang, D. Zhou, H. Xue, S. Zheng, Transplantation of human matrix metalloproteinase-1 gene-modified bone marrow-derived mesenchymal stem cell attenuates CCL4-induced liver fibrosis in rats, Int. J. Mol. Med. 41 (2018) 3175–3184.
[20] N. Itaba, Y. Kono, K. Watanabe, T. Yokobata, H. Oka, M. Osaki, H. Kakuta, M. Morimoto, G. Shiota, Reversal of established liver fibrosis by IC-2-engineered mesenchymal stem cell sheets, Sci. Rep. 9 (2019) 1–12.
[21] T. Liu, P. Wang, M. Cong, D. Zhang, L. Liu, H. Li, Q. Zhai, Z. Li, J. Jia, H. You, Matrix metalloproteinase-1 induction by diethyldithiocarbamate is regulated via Akt and ERK/miR222/ETS-1 pathways in hepatic stellate cells, Biosci. Rep. 36 (2016).
[22] Y. Iimuro, D.A. Brenner, Matrix metalloproteinase gene delivery for liver fibrosis, Pharm. Res. 25 (2008) 249–258.
[23] Y.W. Eom, K.Y. Shim, S.K. Baik, Mesenchymal stem cell therapy for liver fibrosis, Korean J. Intern. Med. 30 (2015) 580.
[24] C.R. Fellows, C. Matta, R. Zakany, I.M. Khan, A. Mobasheri, Adipose, bone marrow and synovial joint-derived mesenchymal stem cells for cartilage repair, Front. Genet. 7 (2016) 213.
[25] O. Onaca, R. Enea, D.W. Hughes, W. Meier, Stimuli-responsive polymersomes as nanocarriers for drug and gene delivery, Macromol. Biosci. 9 (2009) 129–139.
[26] X. Hu, Y. Zhang, Z. Xie, X. Jing, A. Bellotti, Z. Gu, Stimuli-responsive polymersomes for biomedical applications, Biomacromolecules 18 (2017) 649–673.
[27] T. Thambi, J.H. Park, D.S. Lee, Stimuli-responsive polymersomes for cancer therapy, Biomater. Sci. 4 (2016) 55–69.
[28] S. Iqbal, M. Blenner, A. Alexander-Bryant, J. Larsen, Polymersomes for therapeutic delivery of protein and nucleic acid macromolecules: from design to therapeutic applications, Biomacromolecules 21 (2020) 1327–1350.
[29] J. Leong, J.Y. Teo, V.K. Aakalu, Y.Y. Yang, H. Kong, Engineering Polymersomes for Diagnostics and Therapy, 2018.
[30] Y. Zou, M. Zheng, W. Yang, F. Meng, K. Miyata, H.J. Kim, K. Kataoka, Z. Zhong, Virus-Mimicking Chimaeric Polymersomes Boost Targeted Cancer siRNA Therapy In Vivo 29, 2017.
[31] M.A. Yassin, D. Appelhans, R. Wiedemuth, P. Formanek, S. Boye, A. Lederer, A. Temme, B. Voit, Overcoming concealment effects of targeting moieties in the PEG corona: controlled permeable polymersomes decorated with folate-antennae for selective targeting of tumor cells, Small 11 (2015) 1580–1591.
[32] D. Grafe, J. Gaitzsch, D. Appelhans, B. Voit, Cross-linked polymersomes as nanoreactors for controlled and stabilized single and cascade enzymatic reactions, Nanoscale 6 (2014) 10752–10761.
[33] H. Che, S. Cao, J.C.M. van Hest, Feedback-induced temporal control of "Breathing" polymersomes to create self-adaptive nanoreactors, J. Am. Chem. Soc. 140 (2018) 5356–5359.
[34] X. Wang, J. Hu, G. Liu, J. Tian, H. Wang, M. Gong, S. Liu, Reversibly switching bilayer permeability and release modules of photochromic polymersomes stabilized by cooperative noncovalent interactions, J. Am. Chem. Soc. 137 (2015) 15262–15275.
[35] Q. Yan, J. Wang, Y. Yin, J. Yuan, Breathing polymersomes: CO2-tuning membrane permeability for size-selective release, separation, and reaction, Angew. Chem. Int. Ed. 52 (2013) 5070–5073.
[36] Z. Sun, G. Liu, J. Hu, S. Liu, Photo- and reduction-responsive polymersomes for programmed release of small and macromolecular payloads, Biomacromolecules 19 (2018) 2071–2081.

[37] X. Liu, P. Formanek, B. Voit, D. Appelhans, Functional cellular mimics for the spatiotemporal control of multiple enzymatic cascade reactions, Angew. Chem. 129 (2017) 16451–16456.
[38] L.D. Blackman, S. Varlas, M.C. Arno, A. Fayter, M.I. Gibson, R.K. O'Reilly, Permeable protein-loaded polymersome cascade nanoreactors by polymerization-induced self-assembly, ACS Macro Lett. 6 (2017) 1263–1267.
[39] Z. Deng, Y. Qian, Y. Yu, G. Liu, J. Hu, G. Zhang, S. Liu, Engineering intracellular delivery nanocarriers and nanoreactors from oxidation-responsive polymersomes via synchronized bilayer cross-linking and permeabilizing inside live cells, J. Am. Chem. Soc. 138 (2016) 10452–10466.
[40] W. Ke, J. Li, F. Mohammed, Y. Wang, K. Tou, X. Liu, P. Wen, H. Kinoh, Y. Anraku, H. Chen, Therapeutic polymersome nanoreactors with tumor-specific activable cascade reactions for cooperative cancer therapy, ACS Nano 13 (2019) 2357–2369.
[41] O. Rifaie-Graham, S. Ulrich, N.F.B. Galensowske, S. Balog, M. Chami, D. Rentsch, J. R. Hemmer, J. Read de Alaniz, L.F. Boesel, N. Bruns, Wavelength-selective light-responsive DASA-functionalized polymersome nanoreactors, J. Am. Chem. Soc. 140 (2018) 8027–8036.
[42] W. Yang, Y. Xia, Y. Zou, F. Meng, J. Zhang, Z. Zhong, Bioresponsive chimaeric nanopolymersomes enable targeted and efficacious protein therapy for human lung cancers in vivo, Chem. Mater. 29 (2017) 8757–8765.
[43] B.O. Akcora, G. Storm, R. Bansal, Inhibition of canonical WNT signaling pathway by beta-catenin/CBP inhibitor ICG-001 ameliorates liver fibrosis in vivo through suppression of stromal CXCL12, Biochim. Biophys. Acta Mol. basis Dis. 1864 (2018) 804–818.
[44] B.O. Akcora, E. Dathathri, A. Ortiz-Perez, A.V. Gabriel, G. Storm, J. Prakash, R. Bansal, TG101348, a selective JAK2 antagonist, ameliorates hepatic fibrogenesis in vivo, FASEB J. 33 (2019) 9466–9475.
[45] D.W. Kurniawan, R. Booijink, L. Pater, I. Wols, A. Vrynas, G. Storm, J. Prakash, R. Bansal, Fibroblast growth factor 2 conjugated superparamagnetic iron oxide nanoparticles (FGF2-SPIONs) ameliorate hepatic stellate cells activation in vitro and acute liver injury in vivo, J. Control. Release 328 (2020) 640–652.
[46] D. Scholten, J. Trebicka, C. Liedtke, R. Weiskirchen, The carbon tetrachloride model in mice, Lab. Anim. 49 (2015) 4–11.
[47] J. Gaitzsch, D. Appelhans, L. Wang, G. Battaglia, B. Voit, Synthetic bio-nanoreactor: mechanical and chemical control of polymersome membrane permeability, Angew. Chem. Int. Ed. 51 (2012) 4448–4451.
[48] J. Gaitzsch, I. Canton, D. Appelhans, G. Battaglia, B. Voit, Cellular interactions with photo-cross-linked and pH-sensitive polymersomes: biocompatibility and uptake studies, Biomacromolecules 13 (2012) 4188–4195.
[49] R. Ccorahua, S. Moreno, H. Gumz, K. Sahre, B. Voit, D. Appelhans, Reconstitution properties of biologically active polymersomes after cryogenic freezing and a freeze-drying process, RSC Adv. 8 (2018) 25436–25443.
[50] H. Gumz, S. Boye, B. Iyisan, V. Krönert, P. Formanek, B. Voit, A. Lederer, D. Appelhans, Toward functional synthetic cells: in-depth study of nanoparticle and enzyme diffusion through a cross-linked polymersome membrane, Adv. Sci. 6 (2019) 1801299.
[51] A. Lederer, S. Boye, D. Appelhans, Advanced AF4 characterization of dendritic biomacromolecules, their self-assembly, and hybrid formation, in: Recent Progress in Separation of Macromolecules and Particulates, ACS Symposium Series, 2018, pp. 171–187.
[52] F. Ennen, P. Fenner, G. Stoychev, S. Boye, A. Lederer, B. Voit, D. Appelhans, Coil-like enzymatic biohybrid structures fabricated by rational design: controlling size and enzyme activity over sequential nanoparticle bioconjugation and filtration steps, ACS Appl. Mater. Interfaces 8 (2016) 6261–6268.
[53] S. Boye, F. Ennen, L. Scharfenberg, D. Appelhans, L. Nilsson, A. Lederer, From 1D rods to 3D networks: a biohybrid topological diversity investigated by asymmetrical flow field-flow fractionation, Macromolecules 48 (2015) 4607–4619.
[54] H. Gumz, T.H. Lai, B. Voit, D. Appelhans, Fine-tuning the pH response of polymersomes for mimicking and controlling the cell membrane functionality, Polym. Chem. 8 (2017) 2904–2908.
[55] M. Roderfeld, Matrix metalloproteinase functions in hepatic injury and fibrosis, Matrix Biol. 68-69 (2018) 452–462.
[56] F. Xu, C. Liu, D. Zhou, L. Zhang, TGF-β/SMAD pathway and its regulation in hepatic fibrosis, J. Histochem. Cytochem. 64 (2016) 157–167.
[57] R. Omar, J. Yang, H. Liu, N.M. Davies, Y. Gong, Hepatic stellate cells in liver fibrosis and siRNA-based therapy, Rev. Physiol. Biochem. Pharmacol. 172 (2016) 1–37.
[58] S.L. Friedman, Hepatic stellate cells: protean, multifunctional, and enigmatic cells of the liver, Physiol. Rev. 88 (2008) 125–172.
[59] J.E. Puche, Y. Saiman, S.L. Friedman, Hepatic stellate cells and liver fibrosis, Compr. Physiol. 3 (2013) 1473–1492.
[60] F. Ahmed, R.I. Pakunlu, A. Brannan, F. Bates, T. Minko, D.E. Discher, Biodegradable polymersomes loaded with both paclitaxel and doxorubicin permeate and shrink tumors, inducing apoptosis in proportion to accumulated drug, J. Control. Release 116 (2006) 150–158.
[61] M.J. Brol, F. Rösch, R. Schierwagen, F. Magdaleno, F.E. Uschner, S. Manekeller, A. Queck, K. Schwarzkopf, M. Odenthal, U. Drebber, M. Thiele, P. Lingohr, A. Plamper, G. Kristiansen, S. Lotersztajn, A. Krag, S. Klein, K.P. Rheinwalt, J. Trebicka, Combination of CCl(4) with alcoholic and metabolic injuries mimics human liver fibrosis, Am. J. Physiol. Gastrointest. Liver Physiol. 317 (2019) G182–g194.
[62] K. Endo-Umeda, H. Nakashima, S. Komine-Aizawa, N. Umeda, S. Seki, M. Makishima, Liver X receptors regulate hepatic F4/80 (+) CD11b(+) Kupffer cells/macrophages and innate immune responses in mice, Sci. Rep. 8 (2018) 9281.
[63] P. Pakshir, M. Alizadehgiashi, B. Wong, N.M. Coelho, X. Chen, Z. Gong, V. B. Shenoy, C.A. McCulloch, B. Hinz, Dynamic fibroblast contractions attract remote macrophages in fibrillar collagen matrix, Nat. Commun. 10 (2019) 1850.
[64] M.W. Parker, D. Rossi, M. Peterson, K. Smith, K. Sikström, E.S. White, J.E. Connett, C.A. Henke, O. Larsson, P.B. Bitterman, Fibrotic extracellular matrix activates a profibrotic positive feedback loop, J. Clin. Invest. 124 (2014) 1622–1635.
[65] S. Moreno, S. Boye, A. Lederer, A. Falanga, S. Galdiero, S. Lecommandoux, B. Voit, D. Appelhans, Avidin localizations in pH-responsive polymersomes for probing the docking of biotinylated (macro)molecules in the membrane and lumen, Biomacromolecules 21 (2020) 5162–5172.
[66] M.J. Bruining, H.G.T. Blaauwgeers, R. Kuijer, P. Elisabeth, R.M.M.A. Nuijts, L. H. Koole, Biodegradable three-dimensional networks of poly(dimethylamino ethyl methacrylate). Synthesis, characterization and in vitro studies of structural degradation and cytotoxicity, Biomaterials 21 (2000) 595–604.
[67] X.-y. Zhang, P.-y. Zhang, Polymersomes in nanomedicine - a review, Curr. Med. Chem. 13 (2017) 124–129.
[68] Q.Q. Fan, C.L. Zhang, J.B. Qiao, P.F. Cui, L. Xing, Y.K. Oh, H.L. Jiang, Extracellular matrix-penetrating nanodrill micelles for liver fibrosis therapy, Biomaterials 230 (2020) 119616.